Version of Record: https://www.sciencedirect.com/science/article/pii/S0016703722000266
Manuscript_936e8f6988485255d0247b4a35ed4768

Isotope effects at the origin of life: Fingerprints of the Strecker synthesis

Authors: L. Chimiak[a,*], Eiler, J.[b]; Sessions, A. [b]; Blumenfeld, C.[c]; Klatte, M. [d]; Stoltz, B. M.[e]

Affiliations:

[a] Department of Geological Sciences, University of Colorado—Boulder, Boulder, CO, 80309 USA.

[b] Division of Geological and Planetary Sciences, California Institute of Technology, Pasadena, CA, 91125, USA.

[c] Dantari, Inc, Westlake Villiage, CA, 91361, USA.

[d] Dottikon Exlusive Synthesis AG, Dottikon, 5605, CH.

[e] Division of Chemistry and Chemical Engineering, California Institute of Technology, Pasadena, CA, 91125, USA.

*Correspondence to: laura.chimiak@colorado.edu.

Abstract

Strecker synthesis creates α-amino acids from prebiotically plausible substrates (cyanide, ammonia, and aldehydes) and is widely hypothesized to be a key mechanism in the chemistry that led to life on Earth and on other planets. To better constrain the synthetic environments and precursors of abiotic α-amino acids, and to determine unique signatures of abiogenic amino acids, we measured the molecular-averaged and site-specific carbon and nitrogen isotope effects for the Strecker synthesis of alanine. The reaction steps of the Strecker synthesis can be divided into two groups: an initial series of reversible amination and nitrile-addition reactions ('equilibration') and a second series of irreversible hydrolysis reactions ('hydrolysis'). The equilibration of cyanide, acetaldehyde, and ammonia with the intermediate, α-aminopropionitrile (α-APN), has a measured 55.1 ‰ equilibrium nitrogen isotope effect between the ^{15}N-rich amine nitrogen in α-aminopropionitrile and the ^{15}N-poor ammonia and a 20.0 ‰ equilibrium carbon isotope effect between the ^{13}C-poor C-2 site in α-aminopropionitrile and the ^{13}C-rich carbonyl carbon in acetaldehyde. The first irreversible hydrolysis step is inferred to have an up to 10 ‰ normal carbon fractionation (*i.e.,* faster for ^{12}C, slower for ^{13}C) for the whole molecule, but it also has one or more side reactions that deplete the reactive α-APN reservoir by up to 15 ‰. The second hydrolysis step has a 15.4 ‰ normal kinetic isotope effect on the amide (C-1) site of alaninamide, which becomes the carboxyl site of alanine. Other α-amino acids will likely experience similar nitrogen isotope fractionations between ammonia and their amine sites, and similar carbon isotope fractionations between the carbonyl carbon in reactant aldehydes or ketones and the intermediate α-aminonitrile, and between cyanide and the carboxyl site. Therefore, these isotope effects allow us to predict the carbon and nitrogen isotopic contents and intramolecular structures of α-amino acids formed by Strecker synthesis based on their substrates' isotopic compositions,

or to infer the isotopic compositions of substrates from which amino acids formed, for example in the case of the amino-acid-rich carbonaceous chondrites. The site-specific C and N isotopic compositions of amino acids formed by Strecker chemistry contrast with those typical of terrestrial biosynthetic amino acids, so these data also provide a means of discriminating between biogenic and abiogenic α-amino acids.

1. Introduction

Strecker synthesis is one of the simplest routes by which abiotically available precursors produce α-amino acids, the subset of amino acids most prevalent in known life (Masamba, 2021). Specifically, in Strecker synthesis, an aldehyde or ketone reacts with ammonia and cyanide to form an α-aminonitrile that is subsequently hydrolyzed into an α-amino acid (Van Trump, 1975) (Figure 1). Consequently, Strecker chemistry has been hypothesized to have contributed to the prebiotic chemistry that facilitated the origins of life on Earth and potentially in extraterrestrial settings (Miller and Van Trump, 1981; Burton et al., 2012; Fresneau et al., 2015).

The reactants for Strecker synthesis have been detected in the interstellar medium (ISM) and on meteorites (Ehrenfreund and Charnley, 2000; Pizzarello and Shock, 2010). These findings support the hypothesis that Strecker synthesis occurs in the ISM, early solar nebula, and/or meteorite parent bodies. Planetary bodies could be the site of Strecker synthesis through delivery of reactants in meteorites to hydrous environments or through the production of reactants from lighting in planetary atmospheres. The latter occurs in Miller-Urey-style spark-discharge experiments, which simulate lightning in neutral or reduced atmospheres (Miller, 1957; Pizzarello and Shock, 2010).

On meteorites, aldehydes, ammonia, and their potential Strecker synthesis products, α-amino acids, have higher compound-specific H, N and C isotope abundance ratios (*i.e.,* D/H, $^{13}C/^{12}C$ and $^{15}N/^{14}N$) than those observed in common terrestrial materials and in the bulk average (*i.e.*, at hand-sample scale) meteoritic organic matter. These ^{13}C-enrichments decrease with increasing carbon number among the C2+ aldehydes and α-amino acids (Elsila et al., 2012; Aponte et al., 2017; Chimiak et al., 2020). The shared heavy-isotope enrichment and correlation of $^{13}C/^{12}C$ with carbon number have been interpreted as evidence that the meteoritic α-amino acids are derived from the co-occurring Strecker reagents and thus plausibly formed by the Strecker mechanism (Pizzarello et al., 1994; Elsila et al., 2012; Aponte et al., 2017; Simkus et al., 2019). Recent site-specific isotope ratio (SSIR) measurements of an alanine sample from the Murchison meteorite identified a pronounced ^{13}C enrichment that the α-carbon (*i.e.*, $HO_2C\text{-}H\underline{\mathbf{C}}NH_2\text{-}CH_3$), a pattern consistent with derivation by Strecker chemistry from acetaldehyde with a ^{13}C-rich carbonyl carbon (Chimiak et al., 2020). The evidence that Strecker synthesis created α-amino acids in meteorite parent bodies —rocky bodies containing water, simple organics, and (presumably) no life—bolsters its potential as a pathway to form amino acids on early Earth and other planets.

Past experimental and theoretical studies of Strecker synthesis have detailed the effects of physiochemical conditions on its reaction mechanism and kinetics (Ogata and Kawasaki, 1971; Van Trump, 1975; Miller and Van Trump, 1981; Moutou et al., 1995; Atherton et al., 2004;

Yamabe et al., 2014; Magrino et al., 2021). These studies show that Strecker synthesis occurs in the aqueous phase, at basic or acidic pH, and has a water-dependent hydrolysis step (Van Trump, 1975; Moutou et al., 1995). However, despite the importance of the Strecker synthesis to the study of prebiotic chemistry and the role of stable isotope abundances in recognizing its products in natural samples, we are not aware of any prior published studies of isotope effects associated with these reactions. Here we document the carbon and nitrogen isotope effects during Strecker synthesis of alanine, including constraints on site-specific carbon isotope effects. These findings provide a framework for recognizing and quantifying the products of Strecker synthesis in meteorites and other natural samples and environments (*i.e.,* Mars, Europa, or terrestrial hydrothermal systems).

2. Materials and Methods

2.1. Materials

2.1.1. *Strecker synthesis*

All Strecker syntheses performed in this study used the reagents, sodium cyanide (Sigma Aldrich, 97 % purity, Item # 380970, Lot # MKBX0939V), acetaldehyde (>99.5 % purity, Sigma Aldrich, Item # 402788, Lot # SHBG8084V), and ammonium chloride (99.5 % purity, Mallinckrodt Chemicals, Item # 3384-12, Lot # C43615). Ultrapure water– the reaction medium-- was obtained from a MilliPore ultrahigh-purity water system (18.2 MΩ cm; hereafter 'water'). Hydrochloric acid (36.5-38.0 wt. %, Macron Fine Chemicals, Item # 251546) was diluted to produce 6N HCl on the same day as each synthesis.

Strecker syntheses were conducted in heavy-walled 5 mL borosilicate vials (Sigma Aldrich, Item# 29361-U) with new, sterile PTFE stir bars (VWR). Between uses, vials were washed with water and baked at 450 °C to remove organic contaminants. Vials were capped by 20 mm PTFE/Silicone septa (Supelco, 27237-U, lot), which were changed between syntheses. Liquid reagents were added with sterile Luer-lock plastic syringes (BD, multiple lots). Water and acetaldehyde were added with 23-gauge needles (BD, Item# 305145) and HCl was added using a 20-gauge PTFE needle (Aldrich, Z117315) threaded through a 14-gauge needle (Monoject, 2021-01). Holes in septa were sealed with Krytox LVP (Du Pont, Z273546), a non-reactive thermally stable lubricant.

2.1.2. *Purification*

The hydrolysis series in Strecker synthesis produces chloride salts of alanine and alaninamide. These products were desalted on a cation-exchange resin column (AG50W-X8, 100-200 mesh, hydrogen form, Bio-Rad) using 2 M ammonium hydroxide diluted from 28.0-30.0 % (J.T. Baker, *multiple lots)*. Alanine and alanine amide were separated via differential solubility using methanol (MeOH; >99.8 % purity, Macron Fine Chemicals, multiple lots).

2.1.3. *Analytical Standards*

Three alanine standards were used in this study: Alfa Aesar alanine (Purity >99 %), VWR alanine (Purity >99 %, Lot # 2795C477) and one sample of alanine synthesized by us via Strecker synthesis in 2015 (Purity confirmed by NMR).

2.1.4. *Derivatization*

Alanine was derivatized prior to isotopic analysis to enhance its volatility and to enable GC separation and analysis by mass spectrometry with electron impact ionization. Anhydrous methanol (MeOH; >99.8 % purity, Macron Fine Chemicals, multiple lots), n-hexane (>98.5 % purity, Millipore Sigma, HPLC grade, multiple lots), acetyl chloride (AcCl; >99.0 % purity, Sigma Aldrich, Item# 00990, Lot# BCBT8141) and trifluoroacetic anhydride (TFAA; >99 % purity, Sigma Aldrich, Item# 106232, Lot# SHBJ0051) were used to derivatize alanine to alanine-N-trifluouroacetyl-O-methyl ester.

Derivatization reactions were conducted in new, sterile 2 mL borosilicate vials (Microsolv, Item# 9502S-VWC) with new caps. All other glassware used in derivatization was cleaned in DI water and dried in an oven at 450 °C to combust any organics prior to use. Chemical lab syringes (Hamilton, 250 μL) were cleaned with methanol prior to and after derivatization reactions, and instrument inlet syringes (Hamilton, 10 μL) were cleaned with 30 μL hexane before each analysis.

2.2.Methods

2.2.1 Syntheses

Alanine samples were synthesized following methods from Kendall *et al*. (Kendall et al., 1929) modified for the small scale and closed system used in this study. For convenience, throughout this paper we refer to the first step of the Strecker synthesis, which involves relatively low-temperature, mostly reversible reactions among aldehyde, ammonia, and cyanide precursors as the ‘equilibration step,’ and we refer to the second and third steps, which here involve higher temperature hydrolysis of intermediates in an acidic medium, as the ‘hydrolysis series’ (Figure 1).

We note that the hydrolysis series can also occur in basic media (O'Connor, 1970; Van Trump, 1975).

Solid ammonium chloride (approximately 163 mg) and sodium cyanide (approximately 90 mg) were weighed into a reaction vial to which a PTFE stir bar was added. Vials were capped, and 150 µL acetaldehyde and 1 mL water were added separately to the vial via syringe. The puncture site in each reaction vial cap was sealed with Krytox, then vials were put on a stir plate for four hours. Syntheses performed with an initial 'equilibration' step at room temperature (22.5 to 24 °C) sat directly on the stir plate; those at 0 °C were placed in an ice bath on the stir plate; and that at 54 °C was placed in a heated sand bath on the stir plate. Table 1 provides exact amounts of reactants and notes of temperature conditions for each synthesis.

After four hours, samples were removed from the stir plate and hydrolyzed with 6N HCl. To avoid iron contamination from the syringe needles while adding HCl, the 1 mL 6N HCl was measured in a sterile plastic syringe with a PTFE needle attached via the Luer lock. This needle was threaded inside a 14-gauge stainless steel needle to enable puncturing the septum. Both needles entered the vial's cap and headspace together, and the PTFE needle was threaded below the stainless-steel needle before HCl was dispensed into the solution. Krytox was then spread around the exterior needle and, upon removal of the needles, smeared over the opening to prevent gas escape.

For the hydrolysis series, samples were stirred and heated for one hour in a sand bath at temperatures ranging from 80 °C to 120 °C (Table 1). After hydrolysis, samples were removed from heat and bubbled with N_2 via two needles, one to supply nitrogen gas and one to carry away any released gas, including HCN, into a 2M NaOH solution. Needles were attached to the gas lines and to each other with Tygon tubing. Samples were bubbled for 2 minutes after which they were dried under N_2 overnight.

Dried samples were desalted on a Dowex H^+-form 50-100 mesh column using 2M NH_4OH as the eluent, and fractions were collected in test tubes. Each sample fraction was separated via silica gel thin layer chromatography with a mobile phase of 1:1:1:1 1-butanol, ethyl acetate, acetic acid, water solution, and developed with a ninhydrin reagent (1.5 g ninhydrin dissolved in 100 mL 1-butanol and acidified with 3.0 mL glacial acetic acid) to visualize amines (Pirrung, 2007). For a given sample, fractions that tested positive for amines were combined and subsequently dried under nitrogen. Samples were analyzed with proton NMR and liquid chromatography mass spectrometry, which identified alaninamide and alanine as masses 88 and 89 Da respectively. Methanol was added to dried samples, gently shaken, and pipetted into a new vial once particulates had settled to the bottom of the vial. Alaninamide fully dissolves in the methanol layer while alanine remained undissolved. Alanine vials were washed three times in this manner and then both vials were dried under nitrogen.

Four VWR alanine standards with masses 2.3 mg, 5.7 mg, 18.7 mg, and 69.3 mg were processed similarly to a Strecker standard: they were acidified in 1N HCl, dried under nitrogen, and processed through a column and analyzed for $\delta^{13}C_{VPDB}$ as with the Strecker alanine samples. The standards had at least 68 % recovery, and those standards closest in mass to samples (18.7 mg and 69.3 mg) had 87 ± 1 % and 104 ± 5 % recovery from the column. The standards had

$\delta^{13}C_{VPDB}$ values of -20.64 ± 0.09 ‰, -20.74 ± 0.13 ‰, -20.43 ± 0.14 ‰, and -20.45 ± 0.08 ‰, for the 2.3 mg, 5.7 mg, 18.7 mg, and 69.3 mg standards respectively, which are within the error of the unprocessed VWR standard's $\delta^{13}C_{VPDB}$ value of -20.47 ± 0.07 ‰. A 60 mg Alfa Aesar sample following column purification had a C-2 + C-3 $\delta^{13}C$ value of 12.2 ± 2.3 ‰ relative to the Strecker standard which is within error of the C-2 + C-3 site's 13.2 ± 0.4 ‰ value relative to the Strecker standard as found by both Orbitrap measurements and the ninhydrin reaction (see Appendix A). Alanine and alaninamide standards separated by differential solubility in methanol had over 97 % recovery of alanine. Alanine samples were tested for purity via proton NMR.

2.2.2. Isotope Ratio Measurements

Molecular-average $\delta^{13}C$* values of alanine, alaninamide, and sodium cyanide and the $\delta^{15}N$ values of alanine and ammonium chloride were measured on a Thermo Fisher Scientific Flash Elemental Analyzer (EA) coupled to a Delta-V Isotope Ratio Mass Spectrometer (IRMS). Samples were analyzed over a two-day period throughout which standards and blanks were analyzed to calibrate and detect possible drift in the instrument measurements. For $\delta^{13}C$ measurements, measurements of acetanilide standard were interspersed throughout the analysis period and a single measurement of urea and sucrose each occurred at the end of the first day of analysis. Carbon isotope standards had measured $\delta^{13}C_{VPDB}$ values and standard errors of -28.00 ± 0.42 ‰ (acetanilide), -10.98 ‰ (sucrose, 1 measurement), and -27.67 ‰ (urea, 1 measurement), and acetanilide $\delta^{13}C$ values did not drift during the measurement period during which we analyzed alanine and alaninamide samples. These values are within error of recommended values

---

* Delta notation, $\delta^{h}X$, describes the ratio of a heavy isotope of element X (^{h}X) to the light isotope (^{l}X) relative to a standard. It is computed by : $\delta^{h}X = \left[\frac{^{h}R_{sa}}{^{h}R_{st}} - 1\right] \times 1000$ where ^{h}R is equal to the ratio of the heavy-to-light isotope ($\frac{^{h}X}{^{l}X}$) and the delta value is reported in units of per mil (‰).

of -27.7 ± 0.48 ‰ for acetanilide of -27.8 ± 0.1 ‰ for urea, and almost within error of the -10.47 ± 0.13 ‰ value of sucrose. Recommended values for acetanilide and urea were found by calibration against NIST 8542 sucrose standard, which is the sucrose standard measured here.

Measurements of $\delta^{15}N$ were standardized by comparison with a potassium nitrate standard (NIST RM 8549) as well as the alanine and acetanilide working standards. Our measurements of $\delta^{15}N_{AIR}$ for these nitrogen standards had means and standard errors of 3.12 ± 0.13 ‰ (acetanilide) and 5.78 ± 0.16 ‰ (potassium nitrate) during the measurement period, which are 1 ‰ higher than the value published by NIST and those previously measured for acetanilide when it was calibrated to the potassium nitrate standard. All reported data are corrected for that offset by having 1 ‰ subtracted from their measured $\delta^{15}N$ values.

Molecular $\delta^{13}C_{VPDB}$ values of acetaldehyde were measured on a Thermo Fisher gas chromatography-combustion-isotope ratio mass spectrometer (GC-C-IRMS) over the course of one day. A mixture of eight fatty acids (F8 mix) was used to check the instrument's precision prior to acetaldehyde measurements. The method was run with the GC oven isothermal at 80°C and had three on-off pulses of a laboratory tank of CO_2 ($\delta^{13}C$ of -12 ‰) before the sample peak and three after. Acetaldehyde samples were diluted in hexane 1 part in 1000 and manually injected into the GC port. To have three standard CO_2 peaks prior to its elution despite its fast elution time, acetaldehyde samples were injected into the port 180 seconds after the start of the GC method and the inlet port from the GC was vented after the peak's elution to prevent hexane from entering the source.

Techniques for site-specific isotope ratio (SSIR) measurements are outlined in Chimiak et al. (2020) and Eiler et al. (2017); those used here are described in Appendix A. Briefly, alanine was derivatized as the N-trifluoroacetyl-O-methyl ester, diluted to 1:10^5 concentration in hexane, and analyzed on a Thermo Fisher Q-Exactive GC-Orbitrap ('Orbitrap') with a modified inlet system that includes a reservoir to enable trapping and broadening of the eluted GC peak (Figure S1). When the peak for derivatized alanine elutes from the GC it enters the reservoir, from which it is purged by helium over tens of minutes (Figure S3). Each alanine derivative peak was measured for isotope ratios of interest for one hour during which the Advanced Quadrupole Selector mass filtering system—a filtering system that operates similarly to a quadrupole mass spectrometer (Eiler *et al.*, 2017)—was set to pass to the Orbitrap only ions in the window of 135.5 to 145.5 Da. This window permits observation of the 140.031 Da peak ($^{12}C_4H_5ONF_3$) and the 141.035 Da peak ($^{13}C^{12}C_4H_5ONF_3$) which contain the C-2 + C-3 sites in alanine in addition to two carbons from the derivatizing reagent, trifluoracetic anhydride. We report masses of these fragments as reported in the XCalibur Software with no corrections for small calibration errors or the loss of an electron in forming the measured ion. Measurements of the ion intensity ratios of these two peaks ($^{13}R_{sa,meas}$ and $^{13}R_{VWR,meas}$ for the sample and VWR standard, respectively) were converted to $\delta^{13}C_{VPDB}$ values for the average of the sample's C-2 and C-3 sites using equation 1:

$$^{13}R_{corr} = (((^{13}R_{sa,meas}/^{13}R_{VWR,meas} - 1) \text{ x } {}^{nC_{frag}}\!/_{nC_{ala}}) + 1) * {}^{13}R_{VWR,C\text{-}2+C\text{-}3} \qquad \textit{(Eqn.1)}$$

Where the additional variables that appear in Eqn. 1 are: (i) nC_{frag}, the total number of carbon atoms in the measured fragment ion (4 in this case), (ii) nC_{ala}, the numbers of carbons from alanine in that fragment ion (2); and (iii) $^{13}R_{VWR,C\text{-}2+C\text{-}3}$, the $^{13}C/^{12}C$ ratio of VWR alanine in averaged across the C-2 and C-3 sites, which are sampled by the 140.031fragment ion. The $^{13}R_{VWR,C\text{-}2+C\text{-}3}$ value was independently constrained using equation 2 with measured molecular ^{13}R values of this standard via EA-IRMS and measured ^{13}R value of its C-1 site released as CO_2 from ninhydrin decarboxylation and measured on a sector IRMS (See Appendix B).

$$^{13}F_{C\text{-}2\,+\,C\text{-}3} = (3 * {}^{13}F_{molec.} - {}^{13}F_{C\text{-}1})/2 \qquad \textit{(Eqn. 2)}$$

where ^{13}F is the fractional abundance of ^{13}C (*i.e.*, $^{13}C/(^{12}C + {}^{13}C)$), and $^{13}F_{C\text{-}1}$, $^{13}F_{C\text{-}2\,+\,C\text{-}3}$, and $^{13}F_{molec.}$ are the ^{13}F values for the C-1 site, the average of the C-2 and C-3 sites, and full molecule, respectively. Throughout this paper, we perform mass balance calculations involving mixtures of isotopically distinct materials or molecular sites using $^{i}F_{j}$ values rather than $^{i}R_{j}$ or $\delta^{h}X$ values to avoid errors arising from non-linearities in the scales of the latter two (closely related) variables. The $^{i}F_{j}$ values are readily interconverted with $^{i}R_{j}$ or $\delta^{h}X$ values using well established arithmetic relationships.†

After establishing the $\delta^{13}C_{VPDB}$ value averaged across the C-2 + C-3 sites in each sample via equation 1 and determining the molecular-average $\delta^{13}C_{VPDB}$ of each sample via EA-IRMS measurements, solve for the C-1 site's ^{13}C content (which we express below as a $\delta^{13}C_{VPDB}$ value):

$$^{13}F_{C\text{-}1} = 3 * {}^{13}F_{molec.\ avg.} - 2 * {}^{13}F_{C\text{-}2\,+\,C\text{-}3} \qquad \textit{(Eqn. 3)}$$

† $^{i}F_{j}$ is related to $^{i}R_{j}$ by the formula: $^{i}F_{j} = \frac{^{i}R_{j}}{1+\ ^{i}R_{j}}$ and $^{i}R_{j}$ is related to $\delta^{h}X$ as described in footnote *.

As explained in Eiler et al. (2017) and Chimiak et al. (2020), all samples are derivatized with the same reagents and methods, so the derivative-sourced carbons are assumed to have identical $\delta^{13}C$ values between samples and standards and thus only dilute differences in ^{13}C content between a given molecular or fragment species of alanine samples and standards. This assumption was verified by analysis of the differences in isotopic contents between the VWR, Alfa Aesar, and Strecker-synthesis standards by both the mass spectrometric method described here (Appendix A) and previously established values determined by combining EA-IRMS and ninhydrin decarboxylation data for the molecule and C-1, respectively (Eiler et al., 2017; Chimiak et al., 2020). The corroboration of these different methods to calculate the same two sites demonstrates that the derivatization has no significant impact on the C-1 site measurements.

Finally, we note that we compare all standards and samples analyzed over the course of the measurement period. Over the sixteen-day period, the measured ^{13}R values of the VWR alanine standard have no evidence of drift within 2 standard error (Figure S4).

2.2.3. *Calculations of reaction yields*

We directly measured the masses of the cyanide and ammonia and the volumes of the water and acetaldehyde added to the reaction vessel and the masses of the alanine and alaninamide present at the end of the reaction. Consequently, we constrain alanine and alaninamide yields relative to the initial reactants and alanine yield relative to initial alaninamide (*i.e.*, measured alanine + residual alaninamide present at the end of synthesis) from direct measurements. However, the amount of α-APN produced from and residual to the reaction is not directly measured, so yields that involve this factor—that of alaninamide from α-APN and α-APN relative to the reactants—

are constrained using moles of α-APN calculated from the equilibrium reactions. This approach relies on the rapid chemical equilibration, which occurs within minutes (Van Trump, 1975; Atherton et al., 2004) under the conditions used here, between the initial reactants (aldehyde or ketone, cyanide, and ammonia) and their immediate products. Using the methods described in Appendix C, we calculate the equilibrium concentration of α-aminopropanenitrile (α-APN), ammonia, acetaldehyde, and cyanide by solving the system of equilibria between reactants, intermediates, and products depicted in Figure 2 and listed in Table S1.

Following the equilibration step, α-APN is hydrolyzed into alaninamide and then alanine (the second reaction series in Figure 1), both of which are recovered and weighed. Final masses of alaninamide (*i.e.*, the residual alaninamide present at the end of the hydrolysis steps) and alanine were gravimetrically determined. The moles of initial alaninamide are calculated as the sum of the moles of alanine and final alaninamide. The yield of alaninamide from α-APN is calculated as the moles of initial alaninamide divided by the moles of α-APN at equilibrium.

As α-APN is not recovered, we calculate its residual concentration at the end of the hydrolysis steps by taking its calculated concentration after the equilibration step and subtracting the amount converted to alaninamide and any amount that might have been created from or decomposed into the initial reactants (aldehyde, cyanide, and ammonia) during the hydrolysis steps as described in Appendix D.

2.2.4. Calculated isotopic compositions of reaction intermediates

To find isotope effects for each step of the Strecker synthesis of alanine, we calculate the isotope ratios of reactants and products at each step in the reaction depicted in Figure 1. We consider the isotopic composition that a given compound or molecular site can have at four different periods (though most compounds are relevant only to a subset of these): 1) before any reaction ('initial'); 2) when the system ends its 4-hour equilibration ('equilibrium'); 3) at the end of the first hydrolysis step ('H1'); and 4) at the end of the second hydrolysis step ('H2'). Isotope ratio measurements of starting materials, products, and the alaninamide intermediate directly constrain the net carbon and nitrogen isotopic fractionations associated with the Strecker synthesis and of the whole-molecule carbon isotope fractionation associated with the hydrolysis of alaninamide to alanine (H2). Interpreting the net effects as constraints on elementary isotope effects (*i.e.*, isotope effects associated with individual reaction steps) requires a model that considers the isotopic compositions of all intermediates, including those that were not recovered and analyzed for isotopic composition. We use measurements when possible and supplement them with calculations of the quantities and isotopic compositions of reactants, intermediates, and products as described below and in Appendices C-E.

The isotopic compositions of initial reagents, including the $\delta^{13}C$ of the acetaldehyde and sodium cyanide and the $\delta^{15}N$ of the ammonium chloride reactants that were added to the reaction vial, are known from direct measurements. For the equilibrium step, we calculate the $\delta^{13}C$ for all species listed in Figure 2a and $\delta^{15}N$ for ammonia and ammonium and for the amine site of α-APN and α-APN$^+$. We treat the first step as an equilibrium process because the system is closed, and all relevant reactions are reversible on the timescales of our experiments. Consequently, the isotopic compositions of all reacting compounds (and, when relevant, their site-specific isotopic compositions) must be consistent with equilibrium isotope effects (EIEs) among those species, constraints for which are discussed in Appendix E. The reversible reactions permit equilibration between only a subset of sites in each participating molecule: if compounds A and B exist in a chemical equilibrium, the equilibrium step may lead to isotope exchange equilibrium between one site of A and another site of B but not to equilibration of every site in either compound. For the H1 step, we calculate the $\delta^{13}C$ of α-APN and alaninamide, and for the H2 step, we measured the $\delta^{13}C$ of alanine and residual alaninamide and the $\delta^{15}N$ of alanine. Both H1 and H2 are modeled as Rayleigh processes because they are irreversible reactions with associated kinetic isotope effects (KIEs). Compounds and isotope ratios considered in these model calculations are listed in Tables S8 to S11.

Changes in isotope ratios between reactants and products for each step are calculated separately for $\delta^{15}N$, for the molecular-average $\delta^{13}C$, and for the site-specific $\delta^{13}C$ of the C-2 + C-3 sites and of the C-1 sites of α-APN, alaninamide, alanine, and the reactants that form these sites in alanine. We calculate isotope effects for all atomic sites that gain or lose covalent bonds in all elementary reaction steps. This definition includes the nitrogen, C-1, and C-2 sites for the equilibrium step, and the C-1 site for the H1 and H2 steps. We also estimate the molecular-average $\delta^{13}C$ isotope fractionation that results from an isotope effect acting on one or more carbon sites (e.g., if a 9 ‰ effect is estimated for one carbon site of a three-carbon molecule, the corresponding molecule-average fractionation will be 3 ‰). Finally, our analysis considers potential secondary isotope effects for N and the combined C-2 + C-3 sites. At the 2 standard error confidence level no consistent increase or decrease in these secondary sites' isotopic compositions with reaction progress for both H1 and H2; however, we do note that the C-2 + C-3 sites combined averages fluctuate potentially due to fractionations on each site that varies with H1 and H2 in such a way that they cancel out one another.

Appendix E details how the preceding approaches were applied to specific atomic sites and reaction steps.

3. Results

Using the methods described above, we constrained the initial concentrations of reactants and of the final concentrations and yields of alanine and alaninamide. We also measured the molecular-average $\delta^{13}C$ of acetaldehyde and cyanide added to the reaction vessel and of the alanine and alaninamide at the end of the reaction period, the average $\delta^{13}C$ of the C-2 and C-3 sites of the alanine at the end of the reaction period, and the $\delta^{15}N$ of initial ammonium chloride added to the reaction vessel and of the alanine at the end of the reaction period. With these measurements and equations S1 to S14, we calculated the reaction rates and yields and the $\delta^{13}C$ fractionation factors associated with H2 and the overall fractionation between the reactants' $\delta^{13}C$ and $\delta^{15}N$ and the alanine produced at the end of the reactions. Using equations 3 and S18 to S20 (Appendix E), we calculated the carbon and nitrogen stable isotopic compositions of all reactants and intermediates, the carbon isotopic fractionation factors, and the equilibrium and kinetic isotope effects for the equilibration and hydrolysis steps respectively.

3.1. The α-aminopropionitrile formation rates and equilibrium yields

In the initial step of the Strecker synthesis, acetaldehyde, cyanide, and ammonia form and equilibrate with α-aminopropionitrile (α-APN) (Figure 2a). With the kinetics equations from Van Trump (1975), we calculate a forward rate of α-APN production of 1.6 x 10^4 M/hour to 2.1 x 10^4 M/hour for the initial concentrations of the reactive forms of aldehyde, cyanide, and ammonium (*i.e.,* CH_3CHO, CN^-, NH_3; see section 2.2.3, Appendix D, Table 1) present in our reaction vessel at a pH of 5.6 and at the equilibrium pH 8.2, respectively. The average calculated equilibrium concentration of α-APN is 1.7 M, so these rates suggest that equilibrium is achieved on a sub-minute timescale and that at the end of the 4-hour equilibration step, the reactants and intermediates are in equilibrium with one another in all syntheses performed here.

The average proportions of reactants and products for the equilibrium step are depicted in Figure 2a. At the end of the 4-hour equilibration step, the calculated concentration of α-APN produced ranges from 1.79 ± 0.09 mM to 2.23 ± 0.12 mM and residual cyanide, acetaldehyde, and ammonia pools are ~0, 0.38 ± 0.01 mM to 0.85 ± 0.02 mM, and 0.98 ± 0.02 mM to 1.31 ± 0.03 mM, respectively (Table S8). 'Pools' of a compound will refer to all related and rapidly interconvertible forms of that compound; for cyanide this is CN^- and HCN combined, for acetaldehyde it is CH_3CHO and $CH_3CH(OH)_2$ combined, and for ammonia it is NH_3 and NH_4^+ combined. Relative to the cyanide, acetaldehyde, and ammonium pools initially added to the system, the yield of α-APN is 95 % consistently, 62 to 82 %, and 59 to 68 % respectively (Table S9). Therefore, in all syntheses, cyanide is the limiting reagent for the equilibrium step.

Following the equilibrium step, 6N HCl is added to the reaction vessel and α-APN is hydrolyzed into alaninamide and then alanine during the 1-hour hydrolysis period. We evaluate the extent to which this hydrolysis could be accompanied by continued production of α-APN or the degradation of it: significant reactions of this kind would complicate our interpretations of the isotope fractionations associated with reaction steps H1 and H2. To this end, we calculate the maximum rate at which α-APN could be produced by continued reaction among residual cyanide, acetaldehyde, and ammonia during hydrolysis (Appendix D, Equation S15). This rate scales with reactant concentration and temperatures, so to find the maximum rate we use the initial concentrations of acetaldehyde, cyanide, and ammonia rather than that present at equilibrium (which are lower) and the highest hydrolysis temperature (120 °C). These parameters (which overestimate rates for all experiments here), produce a maximum rate of α-APN production of 2.7×10^{-3} M/hr. Similarly, we calculate the maximum rate of α-APN decomposition into its reactants (Appendix D, Equation S16). As the α-APN decomposition rate scales with α-APN concentration and reaction temperature, to find the maximum rate possible in our system, we consider the highest possible α-APN concentration, the amount that would be present if we had quantitative conversion of reactants into α-APN at the 120 °C hydrolysis temperature. With these parameters, the maximum rate of α-APN decomposition (again, an overestimate) is 2.0×10^{-3} M/hr. Based on these calculated rates, during the one-hour hydrolysis, less than 0.2 % of the α-APN at equilibrium would be produced or degraded, which is insignificant to our analysis.

Given that the α-APN production and decomposition after equilibrium are insignificant, we assume the reactants and α-APN reach mutual equilibrium, after which the equilibrium α-APN serves as a reactant pool for the subsequent hydrolysis that occurs following the addition of acid. With this scheme we calculate yields and isotope effects associated with hydrolysis.

3.2. Yields of alaninamide and alanine

Using the calculated quantities of α-APN present after the equilibrium step (Table 1) and the measured amounts of alaninamide and alanine produced in each reaction, we calculated the yields of alaninamide and of alanine. The yield of alaninamide as a fraction of pre-hydrolysis α-APN ranges from 26 % to 89 % and the yield of alanine as a fraction of alaninamide formed by reaction step H1 ranges from 5 % to 100 % (Table S12). Relative to the initial cyanide pool, the yields of total alaninamide and of alanine range from 24 % to 85 % and 2 % to 69 %, respectively (Table S9). The amount of total alaninamide and of alanine produced and their yields positively correlate with each other for temperatures below 115 ºC—excluding one outlier in which all alaninamide was converted into alanine the amounts produced have a correlation coefficient of 0.588 and the yields have one of 0.568 for linear fits.

3.3. Nitrogen isotopes

Measurements of alanine $\delta^{15}N$ values are between 8.8 ‰ and 12.9 ‰ — ^{15}N enriched relative to the initial ammonia pool ($\delta^{15}N = 0.8 \pm 0.3$ ‰, based on measurements of the ammonium chloride reactant). The measured $\delta^{15}N$ of alanine shows no relationship to yield for H1 or H2 (Table S9, Figure S5), suggesting that the amine N does not undergo significant isotopic fraction from H1 and H2, and thus that the amine N site in α-APN has a $\delta^{15}N$ approximately equal to that of alanine. As the α-APN yield is within error for all syntheses, we cannot find a trend with $\delta^{15}N$ of alanine against this parameter.

At equilibrium, roughly two-thirds of the initial ammonia pool is converted to the amine site of α-APN (57 ± 4 % to 68 ± 4 %), while a significant portion remains as ammonia (~3 %) or ammonium (29 ± 1 % to 38 ± 1 %). By mass balance, the residual ammonia pool (including both ammonia and ammonium) is predicted to have a $\delta^{15}N$ value of -17 ‰, nearly 30 ‰ below the alanine value. Given the 29 ‰ EIE between ammonia (^{15}N-poor) and ammonium (^{15}N-rich; Figure 2), the $\delta^{15}N$ of ammonia (*sensu stricu*) at equilibrium lies between -44.69 ± 0.42 ‰ and -42.35 ± 0.37 ‰ (Table S9). The $\delta^{15}N$ of alanine (and thus, we infer, α-APN) is therefore 42.35 ‰ to 57.23 ‰ enriched relative to ammonia, and we infer this reflects the ammonia-α-APN equilibrium nitrogen isotope fractionation (Figure 3, Table S9). The wide range of possible values for this fractionation is due to the anomalous $\delta^{15}N$ of alanine sample 14; barring that sample, this fractionation is calculated to lie between 53.22 ‰ and 57.23 ‰, and we calculate the average $^{15}\varepsilon_{\alpha APN\text{-}NH3}$ at +55.1 ‰.

Our finding that nitrogen isotope KIEs are negligible (~0 ‰) for reaction steps H1 and H2 is expected, as these hydrolysis steps include no bond reordering at the amine nitrogen. Our finding of a large EIE between ammonia and α-APN ($\varepsilon_{aAPN\text{-}NH3}$) during equilibrium (Table 3) can be attributed to the nitrogen bonding environment changing from a lone pair in ammonia to a single bond in α-APN; the latter will have a higher reduced mass at the previously unbonded site, more vibrational states accessible, and therefore a lower vibrational zero-point energy (Li et al., 2021). This equilibrium fractionation is of greater magnitude but the same sign as the 29 ‰ EIE between NH_3 and NH_4^+, in which NH_4^+ with no lone pairs is also ^{15}N-enriched relative to NH_3 with one lone pair. It is also close to the predicted 56.6 ‰ EIE between ^{15}N-poor nitrite and ^{15}N-rich nitrate (Casciotti, 2009) and the experimentally determined $\varepsilon_{NO3/NO2}$ of 60.5 ± 1 ‰ (Brunner et al., 2013).

3.4. Carbon Isotopes

3.4.1. Molecular-Average $\delta^{13}C$

Measurements of the carbon isotope compositions of acetaldehyde and sodium cyanide reagents yield $\delta^{13}C$ values of -26.00 ± 0.13 ‰ and -31.8 ± 0.2 ‰, respectively. Under the simplest assumption that alanine is produced from Strecker synthesis with no isotopic fractionation between reactants and products (or carbon-bearing side products, such as acetaldehyde hydrate), product alanine would have a molecular $\delta^{13}C$ equal to the contribution-weighted average of acetaldehyde and cyanide (2/3 and 1/3, respectively) of -27.9 ± 0.1 ‰. Accounting for the equilibration between acetaldehyde and acetaldehyde hydrate (Figure 2a), for which we use an $\varepsilon_{ace\text{-}ace(OH)2}$ of 4.5 ‰ (Appendix C), the partitioning of modestly ^{13}C-depleted carbon into the acetaldehyde hydrate would lead us to expect a molecular $\delta^{13}C$ of alanine of -27.8 ‰ to -26.7 ‰ (Table S10).

We compute the initial molecular-average $\delta^{13}C$ of alaninamide—that is the value of the entire alaninamide pooled after H1 but before H2—as a concentration-weighted average of the measured molecular ^{13}F values (see Footnote † for definition of ^{13}F) for residual alaninamide and alanine measured at the end of each synthesis, which range from -22.19 ± 0.17 ‰ to -33.63 ± 0.02 ‰ and -27.54 ± 0.16 ‰ to -41.50 ± 0.03 ‰, for residual alaninamide and alanine, respectively (Table S12). Weighted by these abundances (Table S8), the initial molecular $\delta^{13}C$ of alaninamide is calculated to span from -25.8 ± 2.9 ‰ to -39.2 ± 1.1 ‰ (Table S11). These values are strongly correlated with the amide yield from α-APN and weakly correlated with the hydrolysis temperature above 83 ºC (R^2 of a linear regression is 0.356). We calculate the molecular-average $\delta^{13}C$ values of α-APN as the weighted average of the calculated values for the

C-1 site and the C-2 and C-3 sites in α-APN for each synthesis (which are themselves computed based on measured data for reactants; see Appendices C and E). These site-specific values are discussed in the relevant sections below (3.4.2 and 3.4.3, respectively). The molecular average $\delta^{13}C$ value for α-APN computed this way ranges from -26.2 ± 0.5 ‰ to -30.2 ± 0.5 ‰ (Table S11).

The measured $\delta^{13}C$ of alanine produced by Strecker synthesis is between 0.1 ‰ and 14.1 ‰ lower than its alaninamide precursor (Table S11, Figure 4a), which indicates that the overall carbon isotope effect of the Strecker synthesis is 'normal' (*i.e.*, faster for ^{12}C species; slower for ^{13}C species). This finding is bolstered by the fact that the molecular $\delta^{13}C$ of alanine increases (approaching the weighted average of reactants) with increasing yield relative to both starting reactants and the alaninamide intermediate (Figure 4b and c).

The preceding relationships indicate that the estimated α-APN molecular $\delta^{13}C$ values reflect a 6.7 ‰ equilibrium fractionation factor between the ^{13}C-poor α-APN and the more ^{13}C-rich weighted average of cyanide and acetaldehyde (Figure 5a, Table 3). The hydrolysis of α-APN to alaninamide is calculated to have no statistically significant carbon isotope fractionation as the ratio of the calculated residual to initial α-APN ^{13}R values is relatively constant when the fraction of residual α-APN is above 40 % and varies between extremely high and low values (±30 ‰) with no clear trend when the residual α-APN is below 25 % (Figure S6a). We do note an increase in the difference of the molecular average $\delta^{13}C$ of the alaninamide at the end of H1 and of the α-APN at the beginning of H1 (Figure 5b) with high-yield data having values above 0 ‰ (*i.e.*, the alaninamide has a higher $\delta^{13}C$ value than the α-APN). In the highly acidic conditions used here, the α-APN could have undergone side reactions that enriched the α-APN pool available for H1 in $\delta^{13}C$. In this case, at the beginning of H1, α-APN available for reaction would be more ^{13}C-enriched than the value calculated here causing the measured alaninamide $\delta^{13}C$ at the end of H1 to also appear more ^{13}C-enriched relative to the calculated $\delta^{13}C$ value for the α-APN available for reaction. Furthermore, this scenario would mean that fewer mols of α-APN are available for H1 than are calculated and thereby underestimate the calculated yield of alaninamide from α-APN.

The best constrained step, H2, for which $\delta^{13}C$ and abundances of the product alanine and reactant alaninamide are directly measured has a normal 5.2 ‰ kinetic fraction factor (*i.e.*, $\varepsilon_{ala\text{-}amide}$ = -5.2 ‰) (Figure 5c, Table 3).

3.4.2. *The 'amine' and 'methyl' carbon sites of alanine*

The carbonyl and methyl carbons in acetaldehyde become the amine and methyl carbons (the C-2 and C-3 sites, respectively) in alanine (Figures 1 and 2). We measured the molecular average $\delta^{13}C$ values of the initial acetaldehyde and the $\delta^{13}C$ averaged across alanine's C-2 and C-3 sites. Acetaldehyde had a molecular average $\delta^{13}C$ of -26.00 ± 0.13 ‰ Alanine's C-2 and C-3 sites have $\delta^{13}C$ ranging from 3.6 ‰ higher to 8.4 ‰ lower than this value — *i.e.*, from -22.4 ± 1.5 ‰ to -34.8 ± 1.6 ‰ (Table S11). Although the large error in the alanine $\delta^{13}C$ measurements can obscure trends, the data display a clear negative trend between the $\delta^{13}C$ of alanine's C-2 and C-3 sties and hydrolysis temperature for temperatures above 93 ºC (linear fit R^2 = 0.538). As with the nitrogen isotope data, the α-APN yield is within error for most syntheses, so we cannot find a trend against this parameter.

The carbon that ends up in alanine's C-2 site only forms and breaks bonds during the equilibrium step (Figure 2), while the carbon that forms alanine's C-3 site neither forms nor breaks bonds for any step in the reaction (*i.e.,* it is a spectator atom). Neither hydrolysis step demonstrated a trend in $\delta^{13}C$ of the average of these sites with reaction progress (Figures 4b, 4c, and 6b), so we infer that the difference in carbon isotope composition between the initial acetaldehyde and the average of the C-2 and C-3 sites of alanine is predominantly due to an EIE between acetaldehyde's carbonyl carbon and the C-2 site of α-APN. During the equilibrium step, the initial acetaldehyde pool is transformed into a mixture of α-APN (50 ± 6 % to 82 ± 6 %), residual acetaldehyde (70 ± 1 % to 15 ± 1 %), acetaldehyde hydrate (7 ± 1 % to 17 ± 1 %), and α-hydroxypropionitrile (~4 %) (Table S1, Figure 6a). The bonding environments for the C-2 and C-3 carbons in α-APN and α-hydroxypropionitrile are equivalent, so the equilibrium fractionation factor between acetaldehyde and each of these pools is expected to be approximately equal. Consequently, we combine α-APN and α-hydroxypropionitrile into one pool when calculating an EIE between acetaldehyde and α-APN. Using equation S19 (Appendix E) and a value of 1.0045 for $\alpha_{ace\text{-}ace(OH)2}$, we calculate a 10.1 ‰ equilibrium fractionation factor between ^{13}C-enriched acetaldehyde and the ^{13}C-depleted average of α-APN's C-2 and C-3 sites (*i.e.,* this α value = 0.990; Table 3) (Figure 6a). As the C-3 site does not change its bonding environment during this reaction step, we interpret this fractionation as resulting from a 20.0 ‰ EIE between the ^{13}C-enriched acetaldehyde carbonyl carbon and the ^{13}C-depleted C-2 site in α-APN ($\varepsilon_{\alpha APN\text{-}acetaldehyde}$ = -20.0 ‰).

3.4.3. *The 'carboxyl' (C-1) carbon site of alanine*

In Strecker synthesis, cyanide becomes the C-1 site of α-APN, alaninamide, and alanine (Figure 2) as the nitrile carbon, the amide carbon, and the carboxyl carbon, respectively. We measured the $\delta^{13}C$ of the precursor of this site — cyanide — to be -31.8 ± 0.2 ‰, and calculate that of alanine's C-1 site, based on the measured molecular average $\delta^{13}C$ and the measured average $\delta^{13}C$ of the C-2 and C-3 sites, using equation 3 (noting again that all such calculations transform $\delta^{13}C$ values to ^{13}F values prior to such mass balance calculations). Using this method, the $\delta^{13}C$ of alanine's C-1 site ranges from -24.2 ± 3 ‰ to -67.1 ± 3 ‰ with all but two values lying at or below the cyanide pool's value of -31.8 ± 0.2 ‰ (Figure 4, Table S11). These values are only correlated with the moles and yield of alaninamide and alanine.

In the experiments performed in this study, cyanide was nearly quantitatively converted (~95 %, Table S1 and S3) to α-APN's C-1 site during the equilibrium step. Most of the remaining 5 % formed α-hydroxypropionitrile's C-1 site, which has a similar bonding environment to α-APN's C-1 site and therefore is suspected to have a similar EIEs with respect to cyanide. This similarity and the near total conversion of cyanide into α-APN led us to conclude that the $\delta^{13}C$ of the C-1 site in α-APN at the end of the equilibrium reaction step approximately equals that of the starting cyanide, -31.8 ± 0.2 ‰ (Figure 2a, Table S10). Therefore, differences in isotopic composition of the C-1 site of alanine with respect to cyanide reflect isotope effects associated with the hydrolysis series (steps H1 and H2).

As explained above, we infer that alaninamide's average $\delta^{13}C$ for the C-2 and C-3 sites approximately equal those measured in alanine. Consequently, we can calculate the $\delta^{13}C$ of C-1 for alaninamide by subtracting the measured ^{13}F of the C-2 and C-3 sites in alanine from the measured molecular ^{13}F in alaninamide using equation 3 (then converting the resulting ^{13}F value to a $\delta^{13}C$ value for the purposes of reporting; Footnotes 1 and 2). The resulting $\delta^{13}C$ of C-1 for alaninamide ranges from -16.3 ± 3 ‰ to -48 ± 4 ‰ with all but two values within error of or below the $\delta^{13}C$ value of initial cyanide reagent (Figure 4, Table S11). As with alanine, the $\delta^{13}C$ of C-1 for alaninamide only varies with the moles and yield of alaninamide and alanine.

As with the molecular average $\delta^{13}C$ values, the $\delta^{13}C$ of the C-1 site decreases from α-APN to alaninamide to alanine for each synthesis (Figure 4a). Additionally, for each hydrolysis step, the C-1 site's $\delta^{13}C$ approaches that of the reactant cyanide (-31.8 ± 0.2 ‰) with increasing yield (Figure 4b and 4c, Table S11). Both observations indicate a normal KIE acting on the C-1 site of the reactant for the H1 and H2 reactions.

A Rayleigh plot of the evolution of the C-1 $\delta^{13}C$ value with progress of the H1 reaction (which increases from right to left in this figure) yields a trend inconsistent with a single Rayleigh distillation process, implying at least two competing processes during this chemical step (Figure S7c): one process that enriches the α-APN pool available for hydrolysis and the ensuing alaninamide in ^{13}C in a subset of reactions and a second involving normal KIE from hydrolysis that would further enrich the residual α-APN and deplete the alaninamide in ^{13}C. It is reasonable, therefore, to assume that given the evidence for at least two competing fractionations in both the C-1 and the molecular average $\delta^{13}C$ analyses, one or more side reactions during the first hydrolysis step has impacted the calculated yield and fractionation factor for H1.

As with the molecular average $\delta^{13}C$, the $\delta^{13}C$ of the C-1 site has a normal KIE for the hydrolysis of alaninamide to alanine (step H2), and the data are consistent with a single Rayleigh fractionation process ($R^2 = 0.84$) (Figure 7) rather than multiple processes that fractionate the C-1 site like in H1. The H2 step is also the best constrained step with respect to the carbon isotope evolution of the C-1 site because we have made direct measurements of reactant and product abundances and of the $\delta^{13}C$ of the whole product molecule and its C-2 + C-3 sites and of the whole reactant molecule. The normal 15.4 ‰ KIE ($\varepsilon_{ala\text{-}amide}$ = -15.4 ‰) for the C-1 site's hydrolysis from an amide to a carboxyl group in step H2 (Table 3) is roughly three times that of the KIE found for the molecular average $\delta^{13}C$, supporting the idea that the molecular average ^{13}C fractionation for H2 is caused solely by the C-1 site's KIE.

4. Discussion

4.1. Isotope Effects

Recall that the Strecker synthesis can be divided into the three steps depicted in Figure 2: (1) the equilibration between reactants and α-aminonitrile ('Equilibrium'), (2) the hydrolysis of the α-aminonitrile into an α-aminoamide ('H1'), and (3) the subsequent hydrolysis of the α-aminoamide into an α-amino acid ('H2') (Figures 1 and 2). Of these steps, the first occurs in equilibrium and the latter two are irreversible (Van Trump, 1975). In the Strecker synthesis of alanine, we calculate two EIEs for the equilibrium step—an $\varepsilon_{\alpha APN\text{-}NH3}$ of +55.1 ‰ between the ^{15}N-enriched amine site of α-APN and ^{15}N-depleted ammonia and an $\varepsilon_{\alpha APN\text{-}ace}$ of -20.2 ‰ between the ^{13}C-depleted C-2 site of α-APN and the ^{13}C-enriched carbonyl carbon in acetaldehyde—and a normal KIE for H2 of 15.4 ‰ at the C-1 site in alanine ($\varepsilon_{\alpha APN\text{-}CN}$ = -15.4 ‰).

In circumneutral-to-basic hydrolysis conditions, the equilibrium step continues during the hydrolysis steps. The acidic hydrolysis conditions used in this study inhibit significant α-aminonitrile (α-APN) creation or decomposition following the equilibrium step (see Section 3.1). These conditions simplify the reaction pathway such that following the equilibrium step, the α-aminonitrile can be treated as an isolated reactant pool for the irreversible hydrolysis reactions. This simplification permits us to consider each of the three steps independently.

4.1.1. The Equilibrium Step

In the equilibrium step (Figure 2a), two main types of changes occur to convert reactants into product α-APN: (1) lone pairs on nitrogen from ammonia and carbon from cyanide form bonds and (2) the π-bond in acetaldehyde's carbonyl carbon converts into a σ-bond. Prior predictions in which a lone pair on ammonia and cyanide form bonds to create ammonium and hydrogen cyanide, respectively, find that the compound without the lone pair has proportion of heavy-to-light isotopes for nitrogen and carbon, respectively (Urey, 1947). Consequently, we predict that at equilibrium the C-1 and amine sites in α-APN sites will be isotopically enriched relative to ammonia and CN. The isotopic enrichment for the C-1 site would likely be the result of a large isotopic enrichment in the creation of the imine intermediate followed by a smaller secondary isotopic enrichment during the nitrile addition when the amine-bound carbon changes from sp^2 to sp^3 hybridization (Meyer, 2012). Past study on EIEs for addition reactions to carbonyl carbons vary in effect: theoretical work on the hydration of acetaldehyde finds that acetaldehyde hydrate (with two C-OH bonds) is 40 ‰ ^{13}C-enriched relative to acetaldehyde (Hogg, 1980), while an experimental study on CO_2 demonstrates that the product carbonate is 9 ‰ ^{13}C-enriched EIE relative to carbon dioxide (Boettger and Kubicki, 2021). Given that the EIE between the carbonyl carbon and α-APN's C-2 site will depend on the unknown bond frequencies of the C-C and C-N bonds in α-APN relative to those in the C=O bond in acetaldehyde, we cannot predict the EIE. Finally, the methyl carbon on acetaldehyde, which becomes the C-3 carbon in α-APN, is not involved in the reaction, so we expect that its $\delta^{13}C$ value will not change from reactant to product. Future work that produces distinct measurements for the C-2 and C-3 sites is required to confirm this assumption.

Figure 2a displays the measured isotope effects, isotope ratios, and concentrations at equilibrium for reactants, α-APN, and side products. As CN is effectively quantitatively converted into the C-1 site on α-APN and α-hydroxypropionitrile, we cannot measure any EIE for this carbon. The $\delta^{15}N$ measurements agree with the scenario outlined in the preceding paragraph: we find a 55.1 ‰ EIE between of α-APN's ^{15}N-rich amine site and ^{15}N-poor ammonia (Table 3). The calculated EIE is heavily impacted by the 29 ‰ EIE value we used for the reaction NH_3 (*aq*) $\leftrightarrow$ NH_4^+ (*aq*) (Kirshenbaum et al., 1947; Walters et al., 2019). At equilibrium roughly one-third of the initial ammonia pool is in the form of ammonium (29 ± 1 % to 38 ± 1 %) and only 3 % is in the form of ammonia. Because of the high concentration of ammonium relative to ammonia, the ammonium sequesters large amounts of ^{15}N. Errors in this concentration or in the $\varepsilon_{NH4\text{-}NH3}$ value could result in errors in the $\varepsilon_{\alpha APN\text{-}NH3}$. We note that a recent study measured an $\varepsilon_{NH4\text{-}NH3}$ of 45 ‰ (Li et al., 2012) and past studies have found $\varepsilon_{NH4\text{-}NH3}$ values of 20 ‰ (Hogberg, 1997); however, 29 ‰ remains the $\varepsilon_{NH4\text{-}NH3}$ with the clearest consensus in both past and recent theoretical and experiments work (Walters et al., 2019). The 55.1 ‰ EIE we infer agrees with our expectations and is likely due to the stronger bonding environment in the imine and α-APN (no lone pairs) relative to ammonia, which has a lone pair.

In contrast, the equilibrium isotope effect between acetaldehyde's carbonyl carbon and α-APN's C-2 site exhibited an EIE of 20.0 ‰ (Table 3, Figure 6a) that resulted in an ^{13}C-depleted C-2 site on α-APN. As with the ammonia system, the residual acetaldehyde pool is split between two species, acetaldehyde (20 ± 1 % to 15 ± 1 %) and acetaldehyde hydrate (7 ± 1 % to 17 ± 1 %) (Figure 2a, Table S1). As there is no experimentally verified EIE for CH_3CHO (*aq*) ↔ $CH_3CH(OH)_2$ (*aq*), we use values for the hydration of CO_2 (Boettger and Kubicki, 2021), which also involves hydrating a carbonyl carbon, to estimate an approximate $\varepsilon_{ace(OH)2\text{-}ace}$ value of 9 ‰ at the carbonyl site with the acetaldehyde hydrate enriched relative to acetaldehyde. This value could be incorrect especially considering the past theoretic work that estimated $\varepsilon_{ace(OH)2\text{-}ace}$ as high as 40 ‰ at the carbonyl site in equilibrium conditions (Hogg, 1980). Future work that measures the EIE between acetaldehyde and acetaldehyde-hydrate would better constrain our results.

Our measured EIE likely reflects that the C=O bond is stronger than the combined C-C and C-N bonds present α-APN. The magnitude and direction also agree with past studies of amides, thioesters, and oxoesters, which find that the combined EIE between an carbonyl carbon and its sp^3-hydribidzed carbon intermediate and KIE between the sp^3-hydribidzed carbon intermediate the carboxyl product results in a 30 ‰ $\delta^{13}C$ depletion in the product (Robins et al., 2015). Future SSIR work that measures the α-APN intermediate will elucidate the causes for the EIE that leads to a ^{13}C-poor C-2 site in α-APN. If this work was done in at a pH that produced both the lactate and alanine or both α-hydroxypropionitrile and α-APN, one could prove that this bonding environment and not the addition of the imine site leads to the ^{13}C-poor C-2 site in α-APN.

4.1.2. The Hydrolysis series

Following equilibration, α-APN undergoes hydrolysis into alaninamide and then to alanine. These hydrolysis steps are irreversible and occur in a closed system, so associated kinetic isotope effects can be modeled as Rayleigh distillations. The two hydrolysis steps only directly involve the C-1 site in product alanine: in H1, the nitrile is converted into an amide and in H2 the amide is converted into a carboxyl group. These steps are associated with significant bond reordering: during H1, the C-1 site changes hybridization from sp to sp^2, and during H2, the C-1 site changes from sp^2 to sp^3 then back to sp^2. Theoretical and experimental work also suggests indirect involvement of the amine N during the two hydrolysis steps, by stabilizing the water lattice via hydrogen bonding but no involvement of the C-2 or C-3 sites (Yamabe et al., 2014). Given that the hydrolysis steps are irreversible and involve the formation of new bonds only at the C-1 site, we expect a primary normal KIE on the C-1 site for each hydrolysis step and no isotope effects at the C-2 and C-3 sites. While we predict no primary isotope effects on the amine N, due to its potential in stabilizing intermediates we suspect an inverse secondary nitrogen isotope effect on the order of a few per mil could occur.

The model calculations of $\delta^{13}C$ changes for the molecular average and the C-1 site of α-APN during reaction step H1 are inconclusive, suggesting two competing fractionating processes (with one direction dominating early and the other late) and no consistent overall change. These models rely on calculated concentrations and $\delta^{13}C$ values for α-APN and directly measured abundances and $\delta^{13}C$ values for alaninamide. In contrast, our findings provide statistically strong and straightforward support for the expected primary KIEs during reaction step H2 for which both alaninamide and alanine have directly measured concentrations and molecular $\delta^{13}C$ values (Table 3). No significant variations in $\delta^{15}N$ and the average $\delta^{13}C$ of the C-2 and C-3 sites are observed during either hydrolysis step, suggesting they are spectator atoms, as expected (Figures 4b, 4c, 6b, and S1).

During H1, the molecular $\delta^{13}C$ of the product alaninamide and the difference in $\delta^{13}C$ between the reactant α-APN and product alaninamide have overall positive trends with increasing alaninamide yield (Figures 4b and 5b). The C-1 site appears to have these trends, too, although they are obscured by the larger analytical uncertainties for the C-1 measurements (Figures 4b and 7a). The difference between the $\delta^{13}C$ of reactant α-APN and product alaninamide at the C-1 site is at most 15 ‰ with the alaninamide $\delta^{13}C$ lower than the reactant α-APN. However, the difference is only significant for half of the syntheses at high (70 % - 80 %) reaction extents (Figure 5b), and the change in molecular ^{13}R for α-APN versus the fraction of residual α-APN (Figure S7) have trends inconsistent with a single Rayleigh distillation process during this reaction step.

The H1 step's discrepancies from a Rayleigh distillation trend and the potential for opposing isotope effects occurring during H1 lead us to suggest that in some reactions H1 included one or more side reactions that dominated the reaction yield variable. Reaction yield here refers to the fraction of remaining α-APN and was calculated as the difference in the calculated moles of α-APN at the beginning of H1 and the moles of alaninamide present at the beginning of H2 (calculated from directly measured final moles of alaninamide and alanine). If a side reaction consumed α-APN, fewer moles of alaninamide could be made during H1, which would appear in our model as a lower alaninamide yield in H1 and a higher fraction of residual α-APN. If the side reaction had a normal KIE, the α-APN available for hydrolysis would become enriched and product alaninamide would appear more ^{13}C-enriched relative to the α-APN values calculated here, especially when it has high yields (and thus does not express its own KIE as strongly). We suggest that a real understanding of the elementary isotope effects associated with the H1 reaction step of the Strecker chemistry will require direct measurements of the amounts and isotopic compositions of both α-APN and alaninamide, including site-specific effects, and will also require a wider sampling of reaction progress. For these reasons, our considerations of broader implications of this work focus on the more confident conclusions we can reach regarding the equilibrium and H2 steps and the overall net isotope effects of the Strecker chemistry. However, we note the need for future work that starts with α-APN of known site-specific isotopic composition, potentially one that is purchased and hydrolyzed, to better constrain the isotopic fractionations associated with H1.

Data from the H2 step affirm our expectations regarding KIE's associated with hydrolysis. Using the directly measured molecular δ^{13}C values for alaninamide and alanine, we infer a 5.2 ‰ fractionation of the molecular δ^{13}C during H2 (Figure 5c, Table 3) caused by a normal 15.4 ‰ KIE at the C-1 site (Figure 7b, Table 3) (in both cases alanine being ^{13}C-depleted relative to alaninamide). The normal 15.4 ‰ KIE on the C-1 site is roughly thrice that of the molecular average fractionation. We note that in Rayleigh plots (isotope ratio vs. fraction of remaining reactant) for both the molecular and C-1 site carbon isotope values conform to the Rayleigh relationship with high correlation coefficients, suggesting a single mechanism with a constant KIE (Figures 5c and 7b). These facts support the assertion the molecular fractionation associated with converting amide to alanine is solely due the isotope effect associated with hydrolysis at the C-1 site (Figures 5c and 7b). These data also agree with past amide hydrolysis studies, which argue that a normal KIE on a product carboxyl carbon results from the hydroxyl addition to the amide and the ensuing conversion from sp^2 to sp^3 hybridization prior to ammonia leaving (Robins et al., 2015) (Figure 2b).

4.1.3. Non-acidic hydrolysis stage

It is worth nothing that the hydrolysis stage in our experiments take place in highly acidic conditions, which reduces the potential of α-APN dissociation into its reactants (ammonia, acetaldehyde, and cyanide). Natural environments in which this entire reaction would progress in circumneutral to basic conditions would be impacted by the equilibration of α-APN and its reactants even as the irreversible hydrolysis stage progressed. Two key effects could result from this: firstly, the hydrolysis stage would consume α-APN and therefore push the equilibrium between α-APN and its reactants to create more α-APN. In doing so, the overall system would have a greater α-APN yield and therefore α-APN and resulting alaninamide and alanine would have an isotopic composition that more strongly reflects its initial reactant pool (*i.e.*, the alanine would have a more ^{13}C-enriched C-2 +C-3 site and more ^{15}N-depleted amine site relative to the values predicted by this study; effects at the C-1 site would depend on the EIE between cyanide and α-APN).

Secondly, the α-APN pool feeding the hydrolysis stage would consistently equilibrate with the reactants according to the EIEs described in section 4.1. If the H1 fractionation factors are overall normal as suggested in the lowest yields in Figures 6b and 7a, then the hydrolysis stage will result in α-APN with ^{13}C enrichments at both the C-1 and the C-2 + C-3 sites relative to their initial values at the beginning of H1. These values will be more enriched than those dictated by the EIEs with the reactant acetaldehyde and CN. The ^{13}C-enriched α-APN will isotopically equilibrate with the residual acetaldehyde and CN according to their EIEs. As H1 is slower than the equilibrium step, the equilibrations will occur on small amounts of α-APN (rather than the equilibration of compounds described above) and will lower the $^{13}C/^{12}C$ at the C-2 site and possibly at the C-1 site depending on its EIE. As the hydrolysis stage has no significant isotope fractionation associated with nitrogen, this second factor will not impact the nitrogen isotope ratios.

The first effect would lower the $\delta^{15}N$ in the total alaninamide and alanine relative to those measured here and would lead to higher $\delta^{15}N$ values in residual reactant pools than those estimated by our two-stage process. Furthermore, the first effect would increase the $\delta^{13}C$ at the C-2 site in the total alaninamide and alanine relative to those measured here; however, the second effect would decrease it, so the final change in the $\delta^{13}C$ of the C-2 site for the total alaninamide and alanine relative to the values presented in this work would depend on the yield at H1. Conditions that promote a high H1 yield—higher temperatures and more extreme pH—would result in the first effect being dominant and therefore $\delta^{13}C$ at the C-2 site. Conditions that promote a slower H1 step would lead to more competition between the two processes and result in negligible changes at the C-2 site. Analysis on the C-1 site would require measurements of the isotope effects at this site.

4.2. Implications

4.2.1. Abiotic and biosynthetic isotopic fingerprints

For precursors that are similar in $\delta^{13}C$, biological syntheses of amino acids result in carbon isotope structures that differ markedly from those produced by Strecker synthesis, so a measurement of the carbon isotope structure of an amino acid of unknown origin might serve as way to distinguish biotic and abiotic processes. While the experiments here focus on alanine, Strecker synthesis involves the same carbon sites (C-1 and C-2) in all α-amino acids found in biological systems. Consequently, we can assume that the other carbon sites in α-amino acids will behave similarly to the methyl site (C-3) in this study and be spectators to the reaction. The C-1 and C-2 sites on α-amino acids found in biological systems are chemically analogous those in alanine, so it seems likely that when these other α-amino acids are made via Strecker synthesis, they will share similar isotope effects to those measured here.

Studies by Abelson et al. (1961) found that in a variety of photosynthetic organisms grown on non-limited CO_2 alanine's C-1 site is between 0.2 ‰ enriched and 13.8 ‰ depleted in ^{13}C relative to starting carbon sources, that the C-2 and C-3 sites were between 11.8 ‰ and 20.5 ‰ depleted in ^{13}C relative to starting carbon sources, and that relative to the average $\delta^{13}C$ of the C-2 and C-3 sites, the C-1 site was 0.8 ‰ to 15.0 ‰ enriched in ^{13}C (Abelson and Hoering, 1961). For other biosynthetic α-amino acids in the Abelson and Hoering study, most carbon sites were depleted relative to the input carbon and C-1 sites were the most enriched sites in the amino acids.

Our study demonstrates that Strecker synthesis results in a moderate depletion of the averaged C-2 and C-3 sites (up to 16 ± 2 ‰ — an effect we infer primarily results from the equilibration with acetaldehyde) and large ^{13}C depletion at the C-1 site of up to 35 ± 3 ‰ (potentially more under conditions and extents of reaction outside of the range explored here). While in some cases, the molecular $\delta^{13}C$ alone (or the C-1 or the averaged C-2 + C-3 sites $\delta^{13}C$ values alone) could not produce a unique isotopic signature that would readily distinguish Strecker synthesis from the biological production of amino acids, barring large variations in $\delta^{13}C$ values of initial aldehyde and cyanide, Strecker-synthesized alanine will have a C-1 site with lower ^{13}C abundances than that of the weighted average of the C-2 site and the carbons in the side chain, whereas the C-1 sites in biological sources will be ^{13}C-enriched relative to their C-2 site averaged with the side chain. This pattern would be more prominent at lower yields and might be intractable from biological products at high yields in Strecker synthesis (in which case the product alanine's isotope abundances would reflect those of the initial reactants).

The isotopic structures of amino acids produced by Strecker synthesis could approach those previously observed for biological synthesis if the equilibrium step of the Strecker synthesis has relatively low yield and the hydrolysis steps have almost 100 % yields. In this case, assuming similar starting $\delta^{13}C$ values of Strecker reactants acetaldehyde and cyanide, the C-1 site of the product alanine would be higher in $\delta^{13}C$ than the C-2 and C-3 sites, similar to the findings of Abelson and Hoering (1961) for biosynthetic alanine. Thus, the ability of carbon isotope structures to distinguish between Strecker synthesis and biosynthetic origins is clear when hydrolysis yield is low but becomes ambiguous as that yield approaches 100 %.

Prior constraints on the isotopic structures of biogenic amino acids are sparse, and likely inadequate for testing hypotheses regarding the biological origins of these compounds in microbial ecosystems. Future studies should examine site-specific isotope effects in amino acids from a wider range of microbial organisms, including those with metabolic pathways thought to be more closely related to those used by relatively early terrestrial life. One such group of organisms, anaerobic methanotrophic archaea (ANME) (Marlow et al., 2014), has up to 50-60 ‰ normal carbon isotope fractionations between the feedstock carbon—methane or dissolved inorganic carbon—and the ^{13}C-depleted amino acid product (Takano et al., 2018). Takano et al (2018) posit that these fractionations are associated with chain elongation, which should not result in ^{13}C-depleted C-1 site relative to other sites in an amino acid, as seen in Strecker synthesis. However, if these fractionations occur on the C-1 site, they might resemble or exceed those from Strecker synthesis and require revisions in our proposed test of biogenicity. In this case, ^{15}N measurements would be required to better constrain whether the amino acid was produced by Strecker synthesis or biotically.

Strecker synthesis has a marked ^{15}N enrichment in alanine relative to the reactant ammonia and ammonium. Because the mechanism of ammonia addition to the α-carbonyl carbon is the same across all α-amino acids, we anticipate that this effect will also be similar for all α-amino acids created by Strecker synthesis. Isotope fractionations for the microbial assimilation of nitrogen from ammonium into biomass range from -16 ‰ to +1 ‰ and -27 ‰ to 0 ‰, so the biomass is equal to or depleted relative to the initial ammonium for terrestrial and aquatic ecosystems, respectively (Criss, 1999; Sigman et al., 2009) with the phytoplankton *Skeletonema costatum* having the largest fractionation of -27 ‰ (Pennock et al., 1996). These values, especially those in aquatic systems, are both lower in magnitude and opposite in sign to the EIE between ammonium and a Strecker-synthesized α-amino acid's amine site. Starting from the same ammonium supply, therefore, we would anticipate that biological alanine would be ^{15}N-depleted relative to Strecker-synthesized α-amino acids, by up to 53.1 ‰ in a low pH limit (in which the ammonia pool is almost completely ammonium). Relative to the total ammonium pool (ammonium and ammonia combined), the relationship in $\delta^{15}N$ of the pool versus that of alanine is pH dependent. In a low pH scenario, most of the ammonia pool is in an ammonium form and final Strecker-produced alanine will be low, so Strecker synthesized alanine will be 26.1 ‰ more ^{15}N-enriched than the total ammonia pool while amino acids produced by phytoplankton would have fractionations between 1 ‰ enriched to 27 ‰ deplete in ^{15}N relative to the total ammonia pool. In the other extreme, a high pH environment with high yields of alanine from Strecker synthesis, the Strecker synthesized alanine will appear 55.1 ‰ enriched relative to the total ammonia pool and the biotic alanine will be between 2 ‰ and 30 ‰ ^{15}N-enriched relative to the total ammonia pool. Regardless, these differences should be sufficient to distinguish biotic and Strecker-produced α-amino acids (particularly when combined with carbon isotope evidence outlined above) if one can stipulate the $\delta^{15}N$ of the starting ammonium pool.

Some high trophic level organisms could have amino acids with $\delta^{15}N$ similar to those synthesized by Strecker synthesis because $\delta^{15}N$ in amino acids tends to increase with trophic level by 3 to 4 ‰ per trophic level and can increase by up to 8 ‰ per trophic level for glutamate

(Bowes and Thorp, 2015) (Figure 8a). In these organisms, increases in $\delta^{15}N$ tend to occur with only slight (0 to 2 ‰) positive changes in $\delta^{13}C$ per tropic level (Perkins et al., 2014). Therefore, in these cases, the depletions in molecular $\delta^{13}C$ combined with the enrichments in $\delta^{15}N$ in amino acids made by Strecker synthesis could serve as a fingerprint for abiotically synthesized α-amino acids (Figure 3.8b). Here again, inclusion of site-specific carbon isotope measurements will improve this ability to discriminate biotic from abiotic nitrogen isotope signals.

4.2.2. Amino acids in carbonaceous chondrites

It has been previously suggested that Strecker synthesis could be an abiotic route to amino acid formation on carbonaceous chondrite parent bodies and other planetary bodies (Cronin et al., 1993; Pizzarello and Shock, 2010; Burton et al., 2012). This suggestion was recently supported by a study of the site-specific carbon isotope structure of alanine (Chimiak *et al.*, 2020). If this interpretation is correct, we can combine the experimental constraints on N isotope fractionations of the Strecker synthesis presented here with prior measurements of $\delta^{15}N$ values of alanine recovered from the carbonaceous chondrites (Pizzarello et al., 1994; Pizzarello and Holmes, 2009; Pizzarello et al., 2011; Elsila et al., 2012) to estimate a range of $\delta^{15}N$ values for ammonia from which alanine formed (Figure 8a). The predictions agree with independent measurements of the $\delta^{15}N$ of ammonia recovered from Murchison, but underpredict measurements of ammonia from GRA95229 and LAP02342. The discrepancies might reflect the fact that alanine on these two samples formed by mechanisms other than or in addition to Strecker synthesis. Alternatively, the higher residual ammonia $\delta^{15}N$ values could result from continued equilibration with α-APN as the hydrolysis stage progresses as described in section 4.1.3.

5. Conclusions

Strecker synthesis has three main steps: The first is the creation of α-APN which has a 55.1 ‰ nitrogen isotope EIE between reactant ammonia and the ^{15}N-enriched amine site of α-APN and a 20.0 ‰ carbon isotope EIE between the carboxyl site of reactant acetaldehyde and the ^{13}C-depleted C-2 site of α-APN. Isotopic compositions for the amine nitrogen and for the averaged C-2 and C-3 site carbons do not significantly change during hydrolysis of α-APN to alanine.

The hydrolysis of α-APN to alaninamide likely exhibits a normal KIE, but the carbon isotope measurements (molecular-average and site-specific) of this study differ from simple Rayleigh behavior, either because of an uncharacterized side reaction or because of uncertainties in our calculations of progress in the H1 reaction and evolution in $\delta^{13}C$ of α-APN. To better understand the isotope chemistry of the H1 reaction step, future experiments should focus on α-APN hydrolysis alone. However, this uncertainty does not influence our evaluation of the equilibrium isotope effects or the isotope effects associated with H2 to create alanine, or the overall net isotope effects of Strecker synthesis.

The final step in Strecker synthesis (H2) is the hydrolysis of alaninamide to alanine. During H2, the C-1 site undergoes a normal 15.4 ‰ KIE for the conversion of alaninamide to alanine and is the only carbon atom to have a significant isotope effect during this step.

On a molecular level, a consistently depleted $\delta^{13}C$ in conjunction with an enriched $\delta^{15}N$ (relative to reactants) is a signal we document for the Strecker synthesis that is unlikely to be produced biologically. Two conventional measurements—the molecular $\delta^{15}N$ and $\delta^{13}C$ of alanine—give significant ability to forensically determine whether an amino acid was produced by previously studied terrestrial life or by Strecker synthesis. This ability to distinguish biotic and Strecker sources improves further with addition of site-specific carbon isotope data, as the ~15 ‰ depletion of the C-1 carbon relative to the C-2 and C-3 carbons (assuming substrates of approximately uniform $\delta^{13}C$) is a noteworthy signature of alanine produced by Strecker chemistry.

Acknowledgments: We would like to acknowledge Brooke Dallas for her aid in developing the Orbitrap methodology, Dr. David Vander Velde for use of the NMR facilities, and Dr. Scott Virgil for his help in determining the alaninamide intermediate. **Funding:** This project was supported by NASA through LARS grant number NNX17AE52G, by DOE grant DE-SC0016561, by Thermo Fisher, and by the Simons Foundations; **Author contributions:** LC, ALS, and JME designed methods for site-specific carbon isotope measurements. MK, CB, and LC synthesized alanine by Strecker synthesis. BS provided lab space and initial aid in finding a mentor for conducting Strecker synthesis. LC measured isotopic ratios on Strecker synthesized alanine and alaninamide, processed data, calculated concentrations and isotope ratios of intermediates, and calculated predictions of ammonia isotope ratios on meteorites. LC, ALS, and JME contributed ideas to the cause in isotopic deviations at H1; **Competing interests:** Authors declare no competing interests.; and **Data and materials availability:** All data is available in the main text or the Supplementary Information.

Bibliography

Abelson P. H. and Hoering T. C. (1961) Carbon isotope fractionation in formation of amino acids by photosynthetic organisms. *Proc. Natl. Acad. Sci. USA* **47**, 623–632.

Aponte J. C., Elsila J. E., Glavin D. P., Milam S. N., Charnley S. B. and Dworkin J. P. (2017) Pathways to meteoritic glycine and methylamine. *ACS Earth Space Chem.* **1**, 3–13.

Atherton J. H., Blacker J., Crampton M. R. and Grosjean C. (2004) The Strecker reaction: kinetic and equilibrium studies of cyanide addition to iminium ions. *Org. Biomol. Chem.* **2**, 2567–2571.

Boettger J. D. and Kubicki J. D. (2021) Equilibrium and kinetic isotopic fractionation in the CO_2 hydration and hydroxylation reactions: Analysis of the role of hydrogen-bonding via quantum mechanical calculations. *Geochim. Cosmochim. Acta* **292**, 37–63.

Bowes R. E. and Thorp J. H. (2015) Consequences of employing amino acid vs. bulk-tissue, stable isotope analysis: a laboratory trophic position experiment. *Ecosphere* **6**, art14.

Brunner B., Contreras S., Lehmann M. F., Matantseva O., Rollog M., Kalvelage T., Klockgether

G., Lavik G., Jetten M. S. M., Kartal B. and Kuypers M. M. M. (2013) Nitrogen isotope effects induced by anammox bacteria. *Proc. Natl. Acad. Sci. USA* **110**, 18994–18999.

Burton A. S., Stern J. C., Elsila J. E., Glavin D. P. and Dworkin J. P. (2012) Understanding prebiotic chemistry through the analysis of extraterrestrial amino acids and nucleobases in meteorites. *Chem. Soc. Rev.* **41**, 5459–5472.

Casciotti K. L. (2009) Inverse kinetic isotope fractionation during bacterial nitrite oxidation. *Geochim. Cosmochim. Acta* **73**, 2061–2076.

Chimiak L., Elsila J. E., Dallas B., Dworkin J. P., Aponte J. C., Sessions A. L. and Eiler J. M. (2020) Carbon isotope evidence for the substrates and mechanisms of prebiotic synthesis in the early solar system. *Geochim. Cosmochim. Acta*.

Criss R. E. (1999) *Principles of stable isotope distribution*., Oxford University Press on Demand.

Cronin, Chang J. R. and S. (1993) Organic matter in meteorites: molecular and isotopic analyses of the Murchison meteorite.

Ehrenfreund P. and Charnley S. B. (2000) Organic molecules in the interstellar medium, comets, and meteorites: A voyage from dark clouds to the early Earth. *Annu. Rev. Astron. Astrophys* **38**, 427–483.

Eiler J., Cesar J., Chimiak L., Dallas B., Grice K., Griep-Raming J., Juchelka D., Kitchen N., Lloyd M., Makarov A., Robins R. and Schwieters J. (2017) Analysis of molecular isotopic structures at high precision and accuracy by Orbitrap mass spectrometry. *Int. J. Mass Spectrom.* **422**, 126–142.

Elsila J. E., Charnley S. B., Burton A. S., Glavin D. P. and Dworkin J. P. (2012) Compound-specific carbon, nitrogen, and hydrogen isotopic ratios for amino acids in CM and CR chondrites and their use in evaluating potential formation pathways. *Meteorit. Planet. Sci.* **47**, 1517–1536.

Fresneau A., Danger G., Rimola A., Duvernay F., Theulé P. and Chiavassa T. (2015) Ice chemistry of acetaldehyde reveals competitive reactions in the first step of the Strecker synthesis of alanine: formation of $HO–CH(CH_3)–NH_2$ vs. $HO–CH(CH_3)–CN$. *Mon. Not. R. Astron. Soc.* **451**, 1649–1660.

Hogberg P. (1997) Tansley Review No. 95. ^{15}N natural abundance in soil-plant systems. *New Phytol.* **137**, 179–203.

Kendall E. C., McKenzie B. F., Tobie W. C. and Ayres G. B. (1929) dl-Alanine. *Organic Syntheses*, 4–4.

Kirshenbaum I., Smith J. S., Crowell T., Graff J. and McKee R. (1947) Separation of the nitrogen isotopes by the exchange reaction between ammonia and solutions of ammonium nitrate. *J. Chem. Phys.* **15**, 440–446.

Li L., He Y., Zhang Z. and Liu Y. (2021) Nitrogen isotope fractionations among gaseous and aqueous NH_4^+, NH_3, N_2, and metal-ammine complexes: Theoretical calculations and applications. *Geochim. Cosmochim. Acta* **295**, 80–97.

Li L., Lollar B. S., Li H., Wortmann U. G. and Lacrampe-Couloume G. (2012) Ammonium stability and nitrogen isotope fractionations for $–NH_3(aq)–NH_{3(}gas)$ systems at 20–70°C and pH of 2–13: Applications to habitability and nitrogen cycling in low-temperature hydrothermal systems. *Geochim. Cosmochim. Acta* **84**, 280–296.

Magrino T., Pietrucci F. and Saitta A. M. (2021) Step by step Strecker amino acid synthesis from ab initio Prebiotic chemistry. *J. Phys. Chem. Lett.* **12**, 2630–2637.

Marlow J. J., Larowe D. E., Ehlmann B. L., Amend J. P. and Orphan V. J. (2014) The potential for biologically catalyzed anaerobic methane oxidation on ancient Mars. *Astrobiology* **14**, 292–307.

Masamba W. (2021) Petasis vs. Strecker amino acid synthesis: convergence, divergence and opportunities in organic synthesis. *Molecules* **26**.

Meyer M. P. (2012) New applications of isotope effects in the determination of organic reaction mechanisms. *Adv. Phys. Org. Chem.* **46**, 57–120.

Miller S. L. (1957) The mechanism of synthesis of amino acids by electric discharges. *Biochim. Biophys. Acta* **23**, 480–489.

Miller S. L. and Van Trump J. E. (1981) The Strecker synthesis in the primitive ocean. In *Origin of Life* (ed. Y. Wolman). Springer Netherlands, Dordrecht. pp. 135–141.

Moutou G., Taillades J., Bénefice-Malouet S., Commeyras A., Messina G. and Mansani R. (1995) Equilibrium of α-aminoacetonitrile formation from formaldehyde, hydrogen cyanide and ammonia in aqueous solution: Industrial and prebiotic significance. *J. Phys. Org. Chem.* **8**, 721–730.

O'Connor C. (1970) Acidic and basic amide hydrolysis. *Q. Rev., Chem. Soc.* **24**, 553.

Ogata Y. and Kawasaki A. (1971) Mechanistic aspects of the Strecker aminonitrile synthesis. *J. Chem. Soc., B:*, 325.

Pennock J. R., Velinsky D. J., Ludlam J. M., Sharp J. H. and Fogel M. L. (1996) Isotopic fractionation of ammonium and nitrate during uptake by *Skeletonema costatum* : Implications for $\delta^{15}N$ dynamics under bloom conditions. *Limnol. Oceanogr.* **41**, 451–459.

Perkins M. J., McDonald R. A., van Veen F. J. F., Kelly S. D., Rees G. and Bearhop S. (2014) Application of nitrogen and carbon stable isotopes ($\delta^{15}N$ and $\delta^{13}C$) to quantify food chain length and trophic structure. *PLoS One* **9**, e93281.

Pirrung M. C. (2007) *The synthetic organic chemist's companion.*, John Wiley & Sons, Inc., Hoboken, NJ, USA.

Pizzarello S., Feng X., Epstein S. and Cronin J. R. (1994) Isotopic analyses of nitrogenous compounds from the Murchison meteorite: ammonia, amines, amino acids, and polar hydrocarbons. *Geochim. Cosmochim. Acta* **58**, 5579–5587.

Pizzarello S. and Holmes W. (2009) Nitrogen-containing compounds in two CR2 meteorites: ^{15}N composition, molecular distribution and precursor molecules. *Geochim. Cosmochim. Acta* **73**, 2150–2162.

Pizzarello S. and Shock E. (2010) The organic composition of carbonaceous meteorites: the evolutionary story ahead of biochemistry. *Cold Spring Harb. Perspect. Biol.* **2**, a002105.

Pizzarello S., Williams L. B., Lehman J., Holland G. P. and Yarger J. L. (2011) Abundant ammonia in primitive asteroids and the case for a possible exobiology. *Proc. Natl. Acad. Sci. USA* **108**, 4303–4306.

Robins L. I., Fogle E. J. and Marlier J. F. (2015) Mechanistic investigations of the hydrolysis of amides, oxoesters and thioesters via kinetic isotope effects and positional isotope exchange. *Biochim. Biophys. Acta (BBA)-Proteins and Proteomics* **1854**, 1756–1767.

Sigman D. M., Karsh K. L. and Casciotti K. L. (2009) Ocean process tracers: nitrogen isotopes in the ocean.

Simkus D. N., Aponte J. C., Hilts R. W., Elsila J. E. and Herd C. D. K. (2019) Compound-specific carbon isotope compositions of aldehydes and ketones in the Murchison meteorite. *Meteorit. Planet. Sci.* **54**, 142–156.

Takano Y., Chikaraishi Y., Imachi H., Miyairi Y., Ogawa N. O., Kaneko M., Yokoyama Y., Krüger M. and Ohkouchi N. (2018) Insight into anaerobic methanotrophy from $^{13}C/^{12}C$-amino acids and $^{14}C/^{12}C$-ANME cells in seafloor microbial ecology. *Sci. Rep.* **8**, 14070.

Urey H. C. (1947) The thermodynamic properties of isotopic substances. *J. Chem. Soc.*, 562.
Van Trump J. E. (1975) The Strecker synthesis and its prebiological importance. Doctoral dissertation, University of California: San Diego.
Walters W. W., Chai J. and Hastings M. G. (2019) Theoretical phase resolved ammonia–ammonium nitrogen equilibrium isotope exchange fractionations: applications for tracking atmospheric ammonia gas-to-particle conversion. *ACS Earth Space Chem.* **3**, 79–89.
Yamabe S., Zeng G., Guan W. and Sakaki S. (2014) Proton transfers in the Strecker reaction revealed by DFT calculations. *Beilstein J. Org. Chem.* **10**, 1765–1774.

Figures and Tables

Sa	T(°C)		mmol reactants			mmol products	
	EQ	Hyd	CN^-	NH_4^+	ace	amide	ala
1	23	83	2.11	3.32	2.7	1.11	0.47
2	23	83	2.08	3.00	2.7	1.23	0.33
3	23	83	2.02	3.03	2.7	1.26	0.44
4	24	85	1.93	2.90	2.7	1.38	0.89
5	23	83	1.97	2.98	2.7	1.36	1.36
6	24	93	2.12	2.99	2.7	1.29	0.60
7	24	93	2.12	3.00	2.7	1.34	0.47
8	54	95	1.88	3.02	2.7	1.36	0.88
9	23	105	1.95	3.11	2.7	1.47	0.52
10	23	105	2.04	3.08	2.7	1.27	0.27
11	23	105	2.07	3.01	2.7	1.04	0.12
12	25	110	2.00	3.07	2.7	1.15	0.50
13	25	110	1.99	3.07	2.7	1.44	0.84
14	0	110	2.32	3.23	2.7	1.19	0.31
15	0	110	1.94	3.12	2.7	0.88	0.05
16	25	115	2.12	2.99	2.7	1.65	1.14
17	25	115	2.08	2.99	2.7	1.48	0.27
18	25	115	2.21	3.14	2.7	1.87	0.79
19	24	120	1.85	2.94	2.7	0.45	0.12
20	24	120	2.04	3.09	2.7	0.65	0.50

Table 1: Experimental conditions and quantities of reactants and products, in mols. Errors are as follows: 0.5 °C for temperature, 0.02 mmol for initial mmol of cyanide and ammonium, 0.1 mmol for initial mmol acetaldehyde, and 0.01 mmol for final mmol alaninamide and alanine.

Step	Isotope	Site	Value	Comments
EIE	^{15}N		+55.1 ‰	Meas: Concentrations: initial NH_4Cl, final alaninamide and alanine; $\delta^{15}N$: initial NH_4Cl, final alanine Calc: Concentrations: all species at equilibrium, α-APN at the end of H1 $\delta^{15}N$: NH_3 and NH_4^+ at equilibrium Assumptions: No chemical steps other than H1 and H2 occur during hydrolysis, H1 and H2 do not impact $\delta^{15}N$[a]
	^{13}C	Molec Avg	-6.7 ‰	Meas: Concentrations: initial NaCN and CH_3CHO, final alaninamide and alanine; $\delta^{13}C$: initial NaCN and CH_3CHO, final alanine Calc: Concentrations: all species at equilibrium, α-APN at the end of H1 $\delta^{13}C$: α-APN (weighted average of C-1 and C-2 + C-3 values), CH_3CHO, and $CH_3CH(OH)_2$ at equilibrium Assumptions: Same as those for C-2 + C-3 and C-1
		C-2+C-3	-10.1 ‰	Meas: Concentrations: initial CH_3CHO, final alaninamide and alanine; $\delta^{13}C$: initial CH_3CHO, final alanine C-2 + C-3 sites Calc: Concentrations: all species at equilibrium, α-APN at the end of H1 $\delta^{13}C$: CH_3CHO, $CH_3CH(OH)_2$, $CH_3CH(O)CN$ pool at equilibrium Assumptions: CH_3CHO hydration's EIE = CO_2 hydration's EIE, α-APN and $CH_3CH(O)CN$ have the same EIE with respect to CH_3CHO, no chemical steps other than H1, and H2 occur during hydrolysis, H1 and H2 do not impact C-2 + C-3 sites' $\delta^{13}C$[a]
		C-1	N/A	Meas: Concentrations: initial NaCN and CH_3CHO $\delta^{13}C$: initial NaCN Calc: Concentrations: all species at equilibrium Assumptions: α-APN and $CH_3CH(O)CN$ have the same EIE with respect to CN
H2 KIE	^{15}N		0 ‰	Meas: Concentrations: initial NH_4Cl, final alaninamide and alanine; $\delta^{15}N$: initial NH_4Cl, final alanine Calc: α-APN at the end of H1 Assumptions: No chemical steps other than H1 and H2 occur during hydrolysis

Step	Isotope	Site	Value	Comments
H2	^{13}C	Molec Avg	-5.4 ‰	Meas: Concentrations: final alaninamide and alanine; $\delta^{13}C$: final alaninamide and alanine Calc: Initial alaninamide (sum of alanine + alaninamide) Assumptions: Alaninamide and alanine measured represent the H2 step (*i.e.*, no additional loss processes for alaninamide or alanine)
		C-2+C-3	0 ‰	Meas: Concentrations: final alaninamide and alanine; $\delta^{13}C$: final alanine C-2 + C-3 sites Calc: α-APN at the end of H1 Assumptions: no chemical steps other than H1and H2 occur during hydrolysis, H1 and H2 do not impact C-2 + C-3 sites' $\delta^{13}C$[a]
		C-1	-15.4 ‰	Meas: Concentrations: final alaninamide and alanine; $\delta^{13}C$: final alanine C-1 site, final alaninamide molecular Calc: α-APN at the end of H1, $\delta^{13}C$ of initial alaninamide's C-1 site Assumptions: H2 does not impact C-2 + C-3 sites' $\delta^{13}C$[a], alaninamide and alanine measured represent the H2 step

Table 3: Isotope effects for Strecker synthesis. Here positive values denote the product being enriched in the heavy isotope relative to reactants and negative values denote the product being depleted in the heavy isotope relative to reactants. 'Meas' lists quantities that are directly measured and used to evaluate an isotope effect. 'Calc' lists quantities that were calculated (see section 2.2.2.3) and are used to calculate the isotope effect. 'Assumptions' lists assumptions that were made to calculate the isotope effect.

[a]Whether H1 and H2 impact species is determined cross plots of measured isotope ratios vs. reaction progress for each step. If no significant trend in isotope ratio and reaction progress was noted, then we assume no significant KIE was involved.

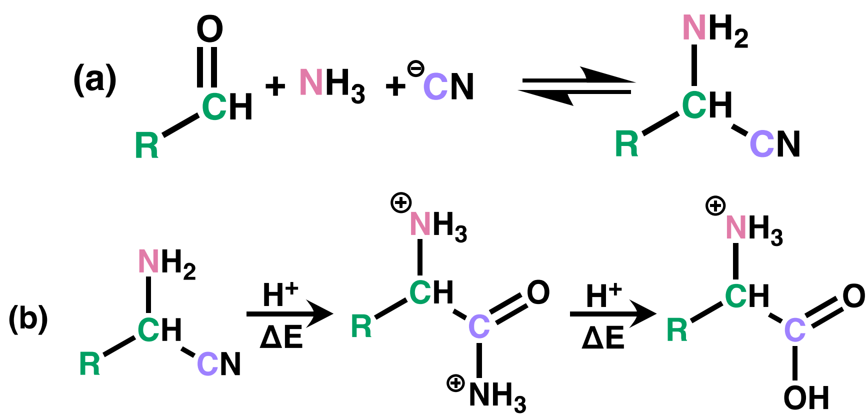

Figure 1: Simplified version of Strecker synthesis. Step (a) is the low temperature equilibrium step. Step (b) comprises the hydrolysis series (H1 and H2). Each hydrolysis step is denoted with the forward arrow.

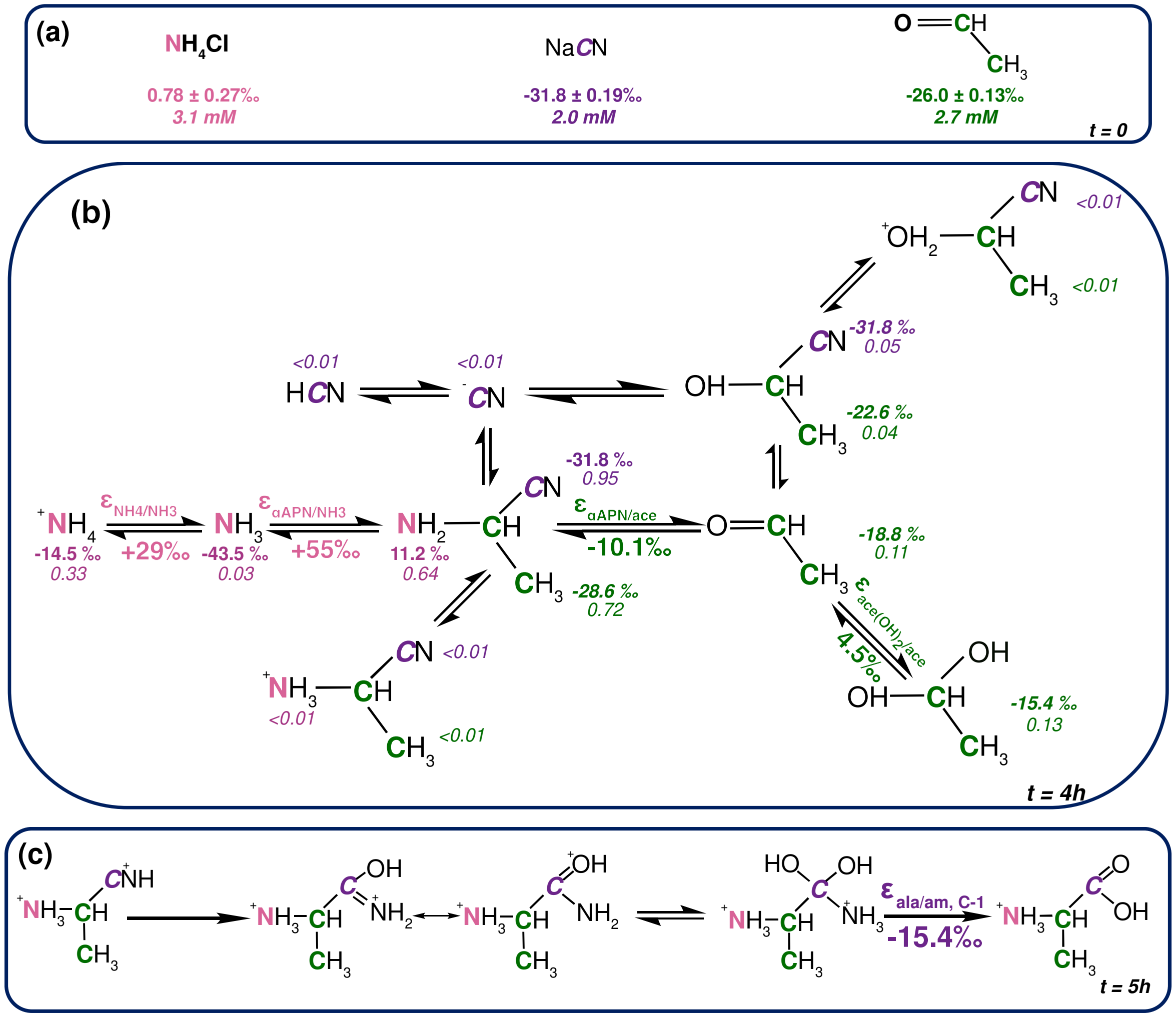

Figure 2: Reactants, mechanisms and associated isotopic partitioning for (a) initial inputs, (b) the equilibrium step, and (c) the two hydrolysis steps in Strecker synthesis. All values in panels (a) are measured, in (b) calculated, and in (c) are calculated from

direct measurements (see section 2.2.3-2.2.4 for details on calculations and direct measurements). Compounds and their corresponding sites in alanine and intermediates are color-coded: nitrogen from the initial NH_4Cl pool is pink, carbon from the initial acetaldehyde in green, and carbon from the initial pool NaCN in purple italics. This color-coding applies to fractionation factors (listed as ε values below the relevant arrow) and other isotopic and concentration information. In panel (b), the equilibrium isotopic compositions are listed under each compound in bold, below which the fraction of the initial compound in each pool is listed in italics. Compounds with less than 0.01 mmol are included for completeness but do not include isotope effects or final isotope values as they are present in such minimal amounts that they do not impact the isotope ratios of the more abundant compounds.

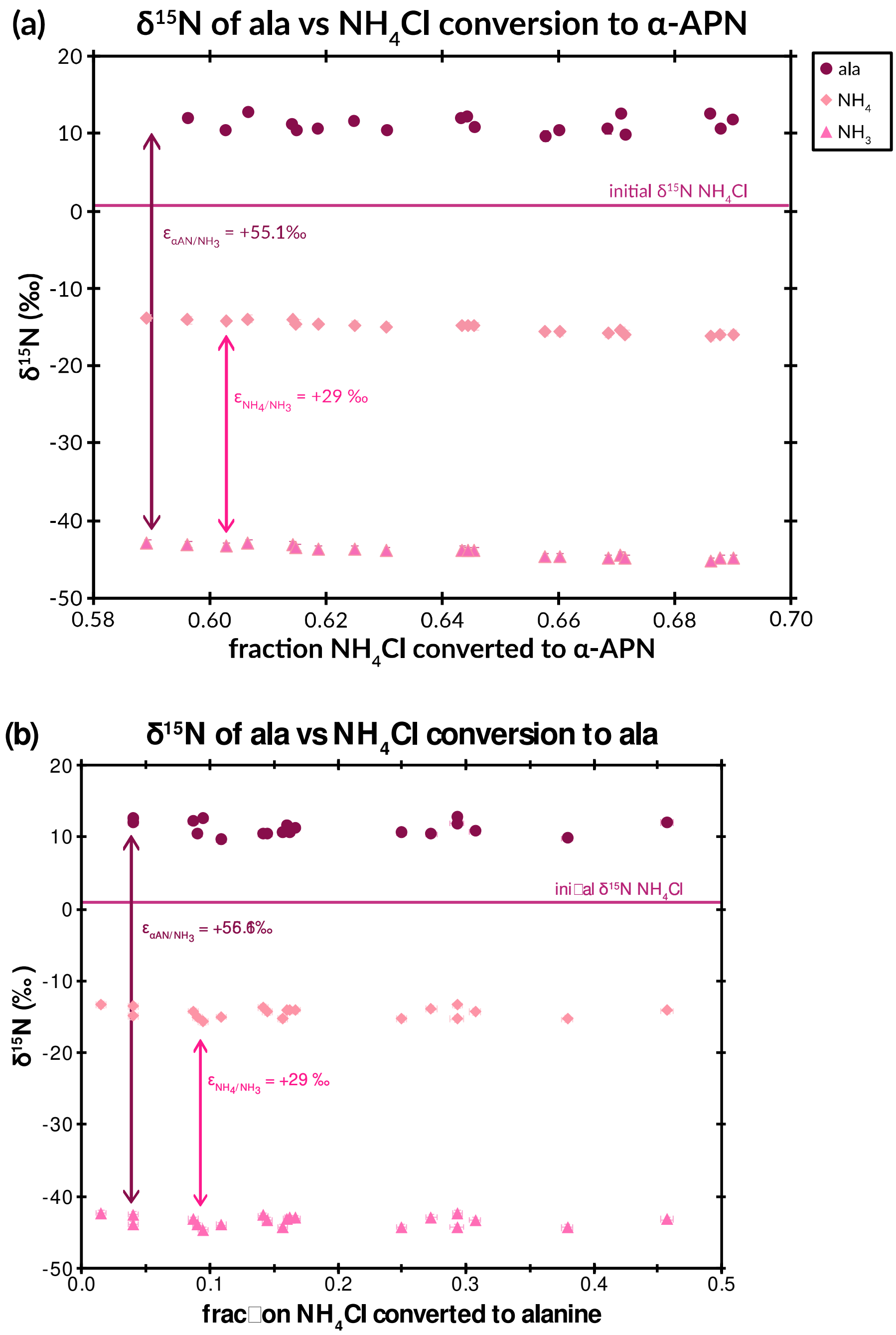

Figure 3: The equilibrium partitioning of nitrogen species plotted relative to the yield of α-APN at equilibrium and the total yield of alanine with respect to initial NH_4Cl input. The initial $\delta^{15}N$ NH_4Cl and the $\delta^{15}N$ of alanine and the fraction of NH_4Cl converted to alanine are measured. The $\delta^{15}N$ of ammonia and ammonium are calculated according to their equilibrium concentrations and that of α-APN. Panel (a) depicts the equilibrium $\delta^{15}N$

values for ammonia, ammonium, and final alanine versus to the α-APN yield at equilibrium and the error of α-APN yield is approximately 6% for all calculations. Panel (b) depicts the same data set relative to the total alanine yield, which has both vertical and horizontal error bars included.

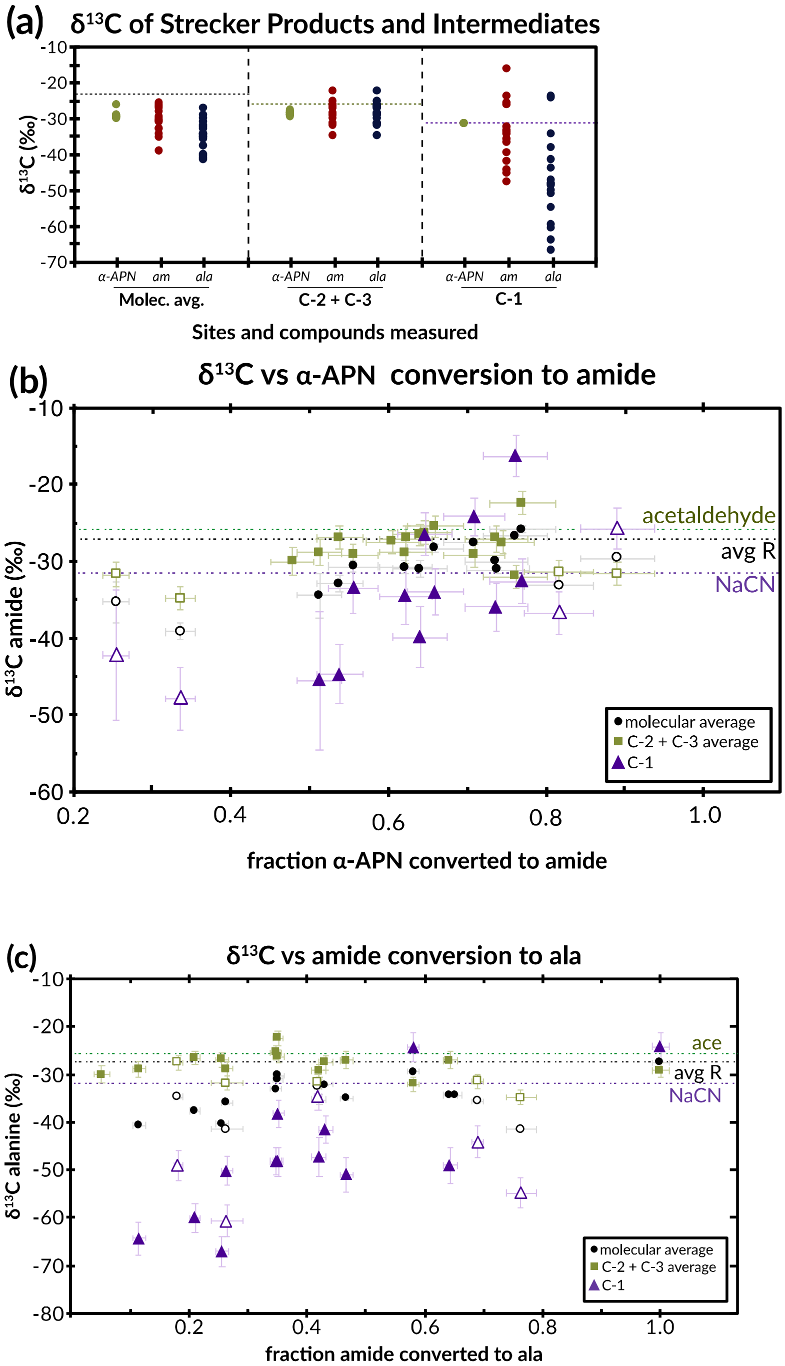

Figure 4: Values of $\delta^{13}C$ for product alanine and intermediates relative to the fraction of initial alaninamide converted to alanine ('fractional conversion'). Panels present carbon isotope compositions of (a) the total amide pool relative to the fractional conversion to amide and (b) alanine relative to the fractional conversion to alanine. All values for intermediates

represent the intermediate pool after formation but before the next reaction (*e.g.*, α-APN $\delta^{13}C$ values represent those after equilibrium and before H1). Both alanine (ala) values are measured, and amide (am) values are calculated as the weighted sum of the measured alanine and amide values, and α-APN values are predicted using the equilibrium concentration calculations and the calculated EIE between acetaldehyde and α-APN. Lines represent the measured $\delta^{13}C$ of the reactants added to the vessel. Molecular and site-specific $\delta^{13}C$ values are plotted against fractional conversion for the hydrolysis steps. Filled symbols represent data from experiments conducted below 115ºC while open symbols are for data from experiments conducted at and above 115ºC.

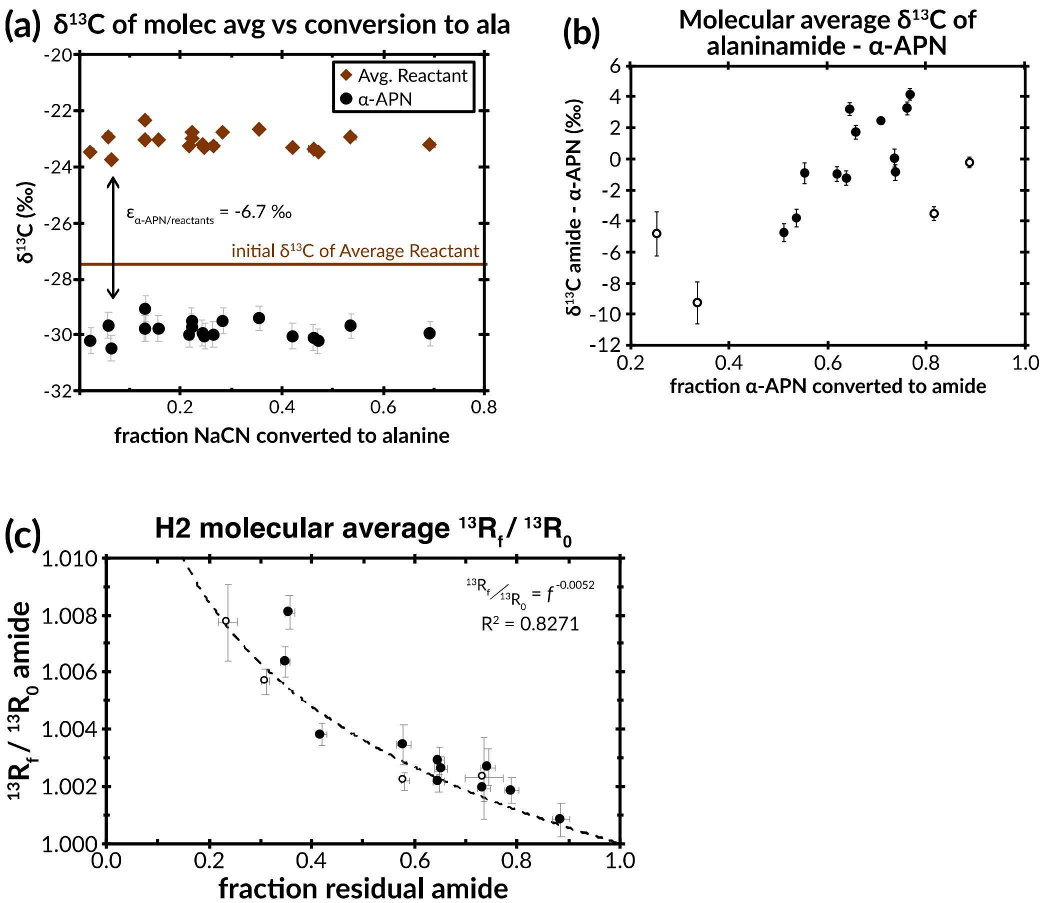

Figure 5: Molecular-average carbon isotope effect models and data. (a) Equilibrium $\delta^{13}C$ values predicted for α-APN and average reactants. Here the $\delta^{13}C$ value represent those at the end of equilibrium but prior to the beginning of H1. (b) The difference between $\delta^{13}C$ values calculated for α-APN at the end of equilibrium and $\delta^{13}C$ calculated from the measured alanine and alaninamide values at the end of H1 but before H2. (c) Ratios of $^{13}R_{residual}$ vs. $^{13}R_{initial}$ for alaninamide versus the fraction of alaninamide remaining after H2. Alaninamide $^{13}R_{residual}$ is measured and $^{13}R_{initial}$ is calculated based on the weighed sums of ^{13}F of alanine and alaninamide collected at the end of H2. In panels (b) and (c), closed circles (●) represent data for alanine in which the hydrolysis series occurs below 115°C and open circles (O) represent data for alanine in which the hydrolysis series occurs at or above 115 °C.

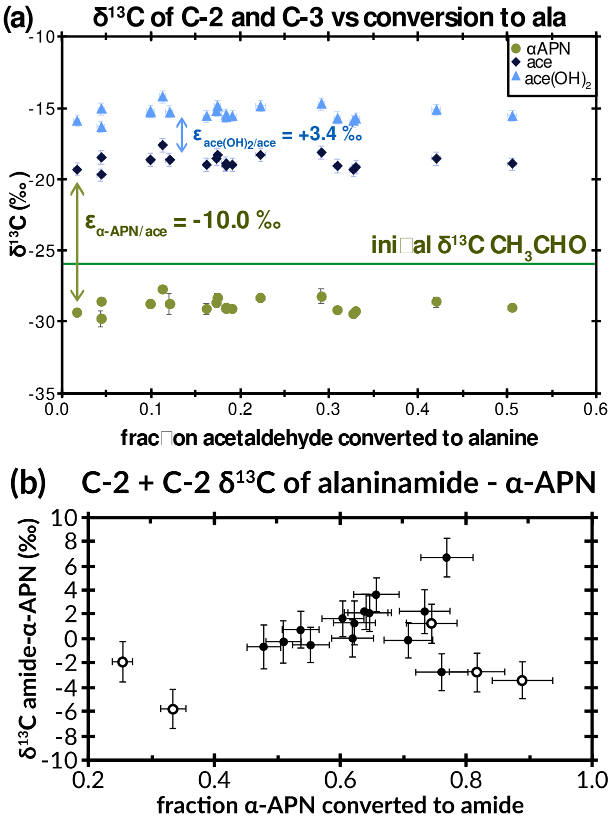

Figure 6: Changes in $\delta^{13}C$ for the C-2 and C-3 sites' average for each step in Strecker synthesis. (a) α-APN $\delta^{13}C$ versus that of acetaldehyde and hydrated acetaldehyde at the equilibrium of reactants and α-APN. (b) Ratio of residual to initial ^{13}R for the C-2 and C-3 site average in α-APN for H1. Closed circles (●) represent data for alanine in which the hydrolysis series occurs below 115 °C and open circles (○) represent data for alanine in which the hydrolysis series occurs at or above 115 °C.

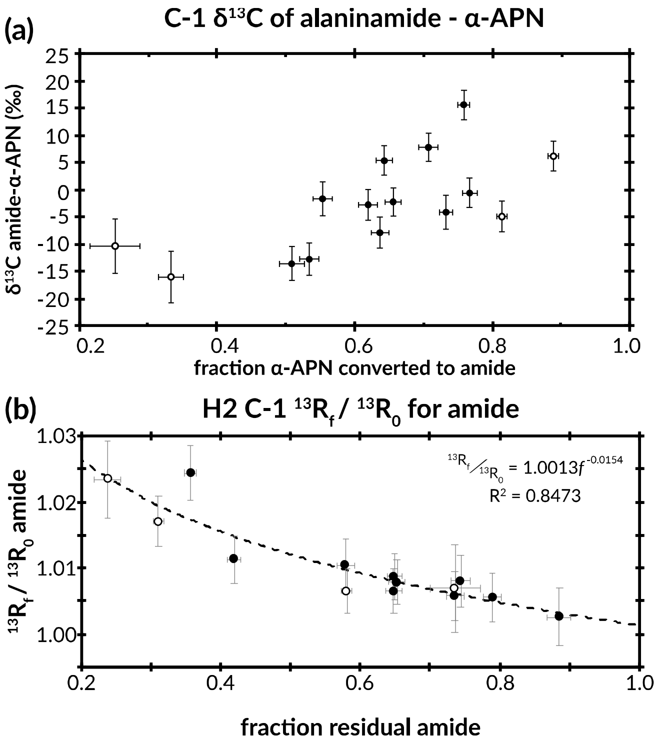

Figure 7: Carbon isotope compositions for the C-1 site. (a)The difference in δ^{13}C between the α-APN reactant and amide product in H1 plotted vs. the progress of conversion of α-APN to amide. Here δ^{13}C of α-APN and the fraction of it converted are calulcted via the equilibrium values from Eqn. S1 to S14. The amide δ^{13}C is calcualted from the weighted sum of the measured δ^{13}C C-1 value of alanine and alaninamide at the end of H2 and assume that the measured δ^{13}C of the C-2 and C-3 sites for alanine have the same values in alaninamide. (b) Ratio of residual to initial ^{13}R for the C-1 site in alaninamide for H2.

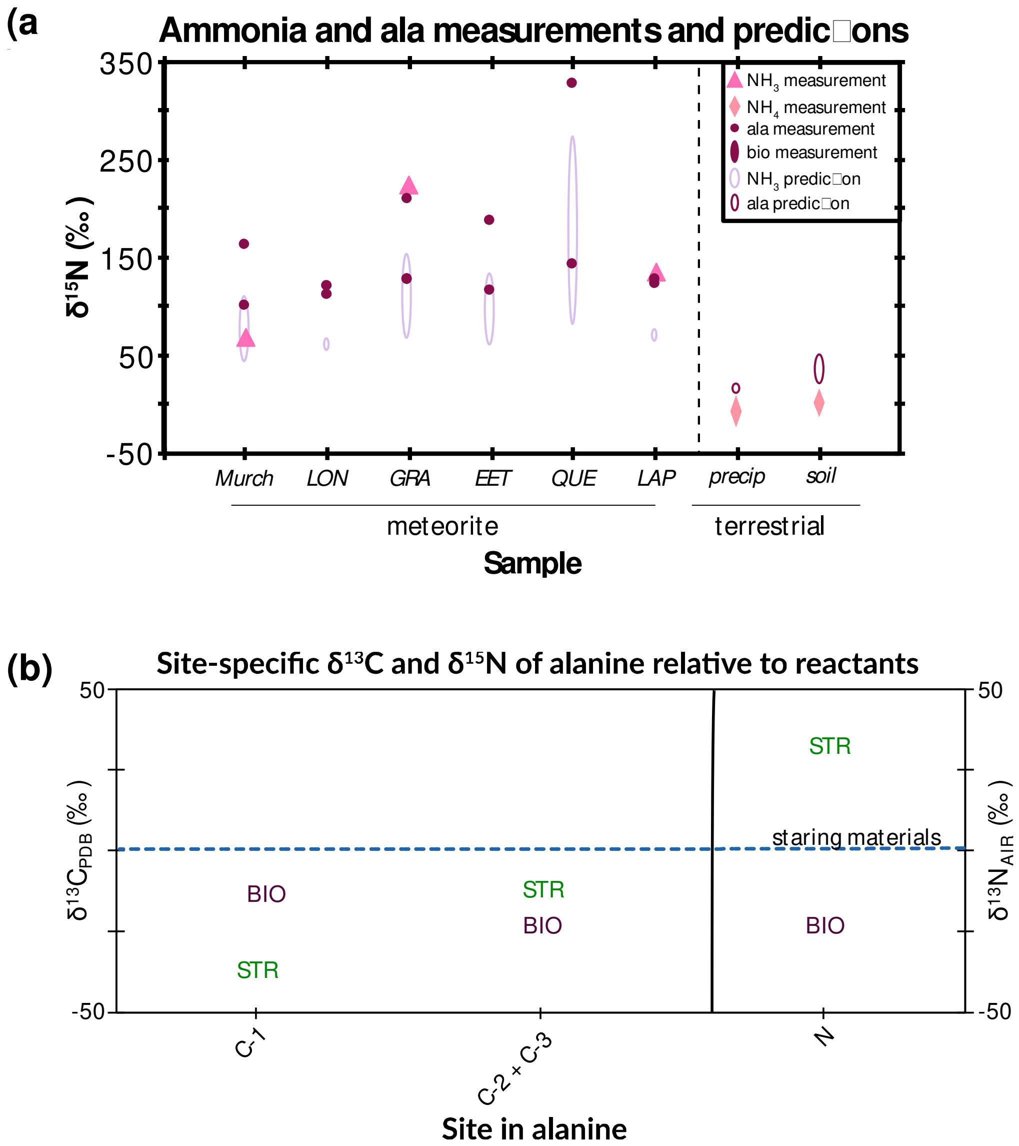

Figure 8: δ^{15}N predictions for ammonia and alanine. (a) δ^{15}N predictions for ammonia on meteorites based on alanine measurements assuming the alanine is produced by Strecker synthesis and predictions for terrestrial alanine produced by Strecker synthesis from precipitation or soil ammonium. On the left, δ^{15}N values of alanine from meteorites (filled burgundy circles) are used to predict possible δ^{15}N ranges ammonia used to synthesize it (open lavender ovals). Where possible, δ^{15}N ammonia measurements from meteorites (filled pink triangles) are included for comparison. On the right, measured

global $\delta^{15}N$ ammonium ranges for precipitation and soil (filled pink diamonds) are used to predict $\delta^{15}N$ alanine (open burgundy ovals). (b) Site-specific $\delta^{13}C$ and $\delta^{15}N$ measurements for Strecker- and biosynthesized alanine relative to input material. The left panel shows $\delta^{13}C$ ranges relative to CN^- and acetaldehyde for C-1 and C-2 + C-3, respectively, for Strecker synthesis (green), and CO_2 for biosynthesis (burgundy) (Abelson and Hoering, 1961). Stars represent alanine biosynthesized in CO_2-limited conditions. The right panel shows $\delta^{15}N$ ranges relative to the input ammonium (not ammonia) for Strecker synthesis and biosynthesis. Biosynthesized data is for all biomass and is from Criss *et al.* (1999) and Sigman *et al.* (2009).